Received 3 November 2025; accepted 16 December 2025. Date of publication 22 December 2025; date of current version 26 March 2026.

Digital Object Identifier 10.1109/OJAP.2025.3646973

Asymptotic Phase Synthesis by Transport Maps—Part I: Theory and Irrotational Linear Maps

PIERO ANGELETTI [1] (Senior Member, IEEE), GIOVANNI TOSO [1] (Fellow, IEEE), AND RAFFAELE VITOLO [2,3]

[1] Radio Frequency Payloads and Technology Division, European Space Agency, ESA/ESTEC, 2201 AG Noordwijk, The Netherlands
[2] Dipartimento di Matematica e Fisica "Ennio De Giorgi," Universita' del Salento, 73100 Lecce, Italy
[3] INFN, Sezione di Lecce, 73100 Lecce, Italy

CORRESPONDING AUTHOR: PIERO ANGELETTI (e-mail: piero.angeletti@esa.int)

The work of Raffaele Vitolo was supported in part by the Research Project Mathematical Methods in Non Linear Physics (MMNLP) by the Commissione ScientificaNazionale—Gruppo 4—Fisica Teorica of the Istituto Nazionale di Fisica Nucleare (INFN), the Department of Mathematics and Physics "E. De Giorgi" of the Università del Salento, GNFM of the Istituto Nazionale di Alta Matematica (INdAM), PRIN 2022TEB52W, "The Charm of Integrability: From Nonlinear Waves to Random Matrices," ICSC–Centro Nazionale di Ricerca in High Performance Computing, Big Data and Quantum Computing, funded by European Union—NextGenerationEU and PRIN2020 F3NCPX "Mathematics for Industry 4.0."

ABSTRACT The paper addresses the problem of phase synthesis of apertures with assigned amplitude. Applying the method of stationary phase it will be shown that the asymptotic solution satisfies a Monge–Ampère partial differential equation (PDE) with appropriate boundary value conditions. In agreement with Chu's energy mapping principle for reflector shaping, the Monge–Ampère PDE can be solved identifying an irrotational transport map from the source aperture to the target beam. After a description of the general theory, the paper focuses on irrotational linear maps associated to quadratic phase solutions demonstrating the possibility of obtaining beams of the same shape of the source aperture, a result only observed for circular and square apertures. Exploiting a polar decomposition of the affine transformation matrix, it will be also demonstrated the possibility of rotating the beam, a result reported (to the best knowledge of the authors) for the first time. In a companion paper, the general problem of finding a solution to the Monge–Ampère PDE via irrotational transport maps will be addressed by mean of the theory of "optimal transport".

INDEX TERMS Phase synthesis, phase-only tapering, spaceborne antennas, array antennas.

I. INTRODUCTION

THE PROBLEM of phase synthesis for apertures with assigned amplitude distribution is of interests in several domains. Early applications involved the shaping of reflector surfaces to obtain cosecant-squared patterns[1] for air surveillance and airborne Radars [1], [2], [3], [4], [5]. With the advent of geostationary satellite technology, the possibility of contouring the spaceborne antenna beam adapting it to the geographical region of interest became of paramount importance, main advantage being the maximization of the gain in the wanted area and minimization of the interference elsewhere. While initially contoured beams were obtained with array-fed reflectors [6], [7], single-feed shaped-reflector technologies [8], [9], [10] emerged as a low complexity/mass/cost solution that gained commercial dominance for single-beam broadcasting antennas [11]. In all these applications the connection between reflector surface shaping and the phase synthesis problem is due to the fact that a first-order approximation of the surface variation can be interpreted as a phase variation of the projected aperture field/current [12], [13].

During the Cold War, the deployment of Inter-Continental Ballistic Missiles (ICBMs) created a compelling need for Radar systems with greater detection ranges superseeding the peak power limitation imposed by the radar equation. With the development of Radar pulse compression, phase synthesis took the form of the problem of designing a signal of arbitrary envelope having a specified spectral magnitude and hence, a specified autocorrelation function [14], [15], [16], still a subject of active research [17].

[1] With range-independent echo return for targets at constant altitude.

More recently, the phase synthesis problem gained increasing interest in reflect-array design and active array applications, where the use of constant amplitude excitations permits to operate the amplifiers feeding the radiating elements at maximum efficiency. In this last context the problem is also known as "phase-only" synthesis. Being the array (or the reflect-array) composed of a discrete number of elements, the optimization problem is of discrete nature, and several approaches have been proposed. Methods originally developed for continuous waveforms [15], [16] and reflectors [1], [2], [3], [4] design have been applied to linear [18], [19] and planar arrays [20]. A wide variety of local and global numerical optimization methods have been applied to the discrete problem. Among the local methods it is worth mentioning early steepest descent methods [21], [22], the method of alternating projections [23] (which has been equipped with fast projectors based on the Non-Uniform Fast Fourier Transform - NU-FFT [24]), and integral equations methods [25], [26]. A non exhaustive list of contributions to the phase-only synthesis problem with global numerical optimization methods includes: genetic algorithm (GA) [27], [28], particle swarm optimization [29], [30], Taguchi's method [31], cross entropy method [32], and invasive weed optimization [33].

This last contribution [33] demonstrated that the phase-only synthesis of large planar arrays (a discrete problem) can be efficiently addressed solving the continuous phase synthesis problem on the aperture of the array and sampling the solution at the elements position, a general result which is independent of the adopted optimization technique. In this perspective, techniques initially developed to solve the continuous aperture problem of reflector shaping or pulse compression can be applied to the discrete phase-only problem.

Among the approaches with highest "explanatory power", Chu's method [3] interprets the synthesis of a shaped beam on the base of a fundamental principle of conservation of energy. The phase variation acts as a mapping of the energy from the aperture to the far-field. The mathematical explanation of this concept is founded on the asymptotic approximation of the Fourier integral [34] by means of the principle of the stationary phase [35], [36], [37], [38], [39], [40], [41], [42], [43]. The mathematical details were elaborated by Dunbar [5] and later by Fowle [16] for linear apertures and pulse compression, respectively. An extension of the mapping approach to the bidimensional case was first proposed by Katagi and Takeichi [10] which suggested to construct a wavefront corresponding to the desired beam shape and then use geometrical optics to shape the reflector, a technique known as "wavefront synthesis" [12]. As highlighted by Nomoto [44] for the specific case of fan-beams, the arbitrariness in the selection of the wavefront mapping is equivalent to a lack of total differentiability conditions which degrades the quality of the performance. In this respect, aperture synthesis provided a more direct link to performance [13]. In parallel to the

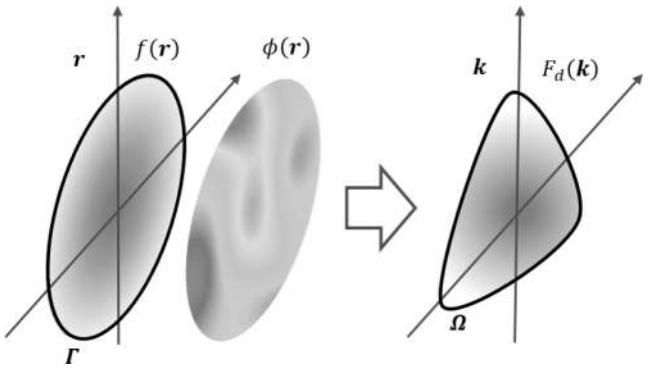

FIGURE 1. Problem description.

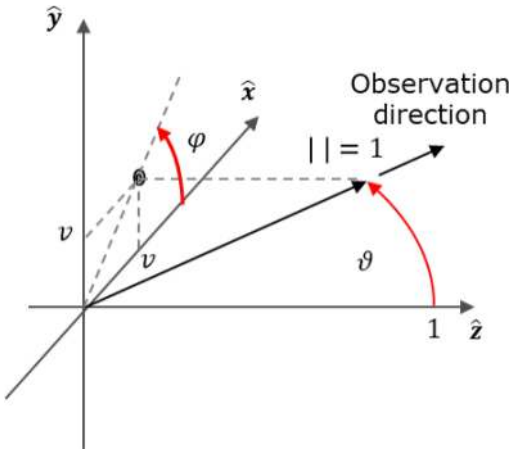

FIGURE 2. Geometry.

intuitive methods of wavefront synthesis, more sofisticated geometrical optics formulations of the reflector shaping problem were developed as a boundary value problem of a partial differential equation of the Monge–Ampère type [45], [46], [47].

In the following we will first demonstrate that direct application of the method of stationary phase to a planar aperture distribution provides an exact formulation of the bidimensional phase synthesis problem, casting the solution in a Monge–Ampère partial differential equation [48], [49], [50], [51] complemented with appropriate boundary value conditions [52], [53]. The phase synthesis problem can so be translated in the search of an irrotational transport map from the source aperture to the target beam, in agreement with Chu's energy mapping principle, in line with the wavefront synthesis interpretation, and ensuring total differentiability.

Making use of irrotational linear maps we will derive a simple quadratic solution which demonstrates the possibility of obtaining beams of the same shape of the source aperture, results which have been already observed for circular [20] and square [54], [55] apertures. We will further demonstrate possibility to rotate the beam exploiting a polar decomposition of the affine transformation matrix, a result reported in this paper (to the best knowledge of the authors) for the first time.

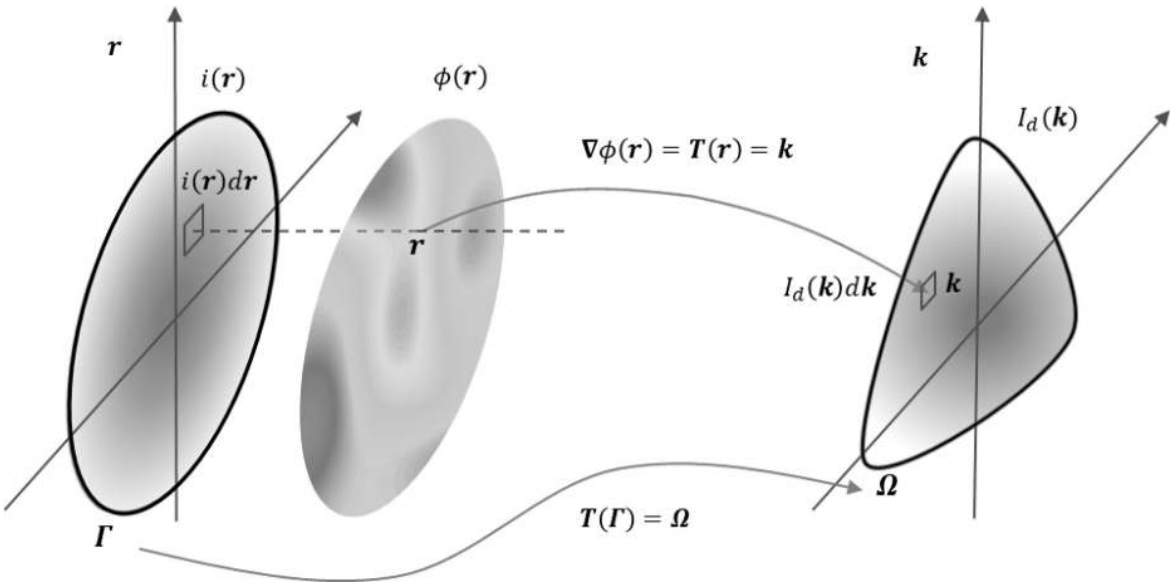

FIGURE 3. Phase Synthesis as a Transport Map Problem.

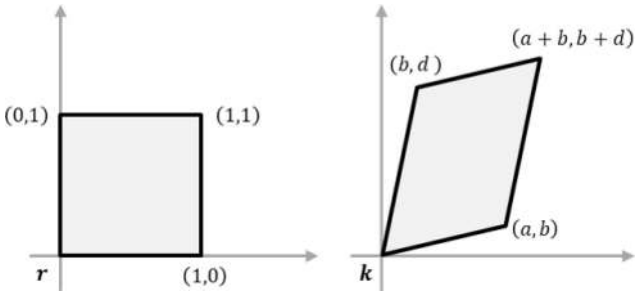

FIGURE 4. Symmetric Affine Transformation Diagram.

The solution will be generalized to arbitrary shapes of the source aperture and target beam by mean of the theory of "optimal transport" [56] in a subsequent part II paper [57].

The paper is organized as follows: Section II describes the mathematical problem and how the application of the method of stationary phase leads to a PDE of the Monge-Ampère type. General details of the Monge-Ampère PDE for the intensities is discussed in Section III. The link between Monge-Ampère PDE and irrotational transport map problem is elaborated in Section IV, and results related to irrotational linear transport maps, together with an overview of related results in Section V. Conclusions follow.

II. BIDIMENSIONAL STATIONARY PHASE METHOD AND MONGE-AMPÈRE PARTIAL DIFFERENTIAL EQUATION

The phase synthesis problem can be described as the problem of determining the phase distribution $\phi(\boldsymbol{r})$ over the planar aperture domain $\boldsymbol{\Gamma}$, with assigned real amplitude distribution $f(\boldsymbol{r})$, such to obtain a far-field distribution with desired magnitude $F_d(\boldsymbol{k})$ over the target beam domain $\boldsymbol{\Omega}$ (Fig. 1).

In the scalar far-field approximation, the radiation pattern of a linear continuous aperture is given by the Fourier transform of the aperture field:

$$F(\boldsymbol{k}) = \mathcal{F}\left(f(\boldsymbol{r})e^{j\phi(\boldsymbol{r})}\right) = \\ = \iint_{\boldsymbol{\Gamma}} f(\boldsymbol{r})\, e^{j\phi(\boldsymbol{r})}\, e^{-j\,\boldsymbol{k}\cdot\boldsymbol{r}}\, d\boldsymbol{r} \tag{1}$$

with,

$$\boldsymbol{r} = \begin{bmatrix} x \\ y \end{bmatrix}, \quad \boldsymbol{k} = k_0 \begin{bmatrix} u \\ v \end{bmatrix}, \tag{2}$$

where $k_0 = 2\pi/\lambda$ is the free-space wavenumber and relevant coordinate systems are depicted in Fig. 2 and satisfy the following relationships

$$u = \sin(\vartheta)\cos(\phi), \quad v = \sin(\vartheta)\sin(\phi), \\ \vartheta = \sin^{-1}\sqrt{u^2+v^2}, \phi = \tan^{-1}\left(\frac{v}{u}\right). \tag{3}$$

Phase Synthesis Problem - Assigned the real positive magnitudes $f(\boldsymbol{r})$, $\boldsymbol{r} \in \boldsymbol{\Gamma}$, and $F_d(\boldsymbol{k})$, $\boldsymbol{k} \in \boldsymbol{\Omega}$, find the phase distribution $\phi(\boldsymbol{r})$ such that: $|F(\boldsymbol{k})| \approx F_d(\boldsymbol{k})$

The asymptotic approximation for the field, determined by the limit $\lambda \to 0$ in the Fourier integral (1), is mathematically analogous to the high-frequency limit of the wave equation. This limit, derived classically via the *Luneburg–Kline expansion*, yields the well-known *eikonal* and *transport equations* [58]. While these ray-optical methods are fundamentally suitable for modeling propagation in the *near-field* or for *finite-to-finite surface problems* (e.g., reflector shaping), our specific application is *aperture-to-far-field* synthesis. We utilize this asymptotic framework here not for propagation modeling, but to establish the rigorous power conservation principle (flux preservation) between the aperture domain $\boldsymbol{\Gamma}$ and the distant angular domain $\boldsymbol{\Omega}$. This conservation law, derived from the stationary

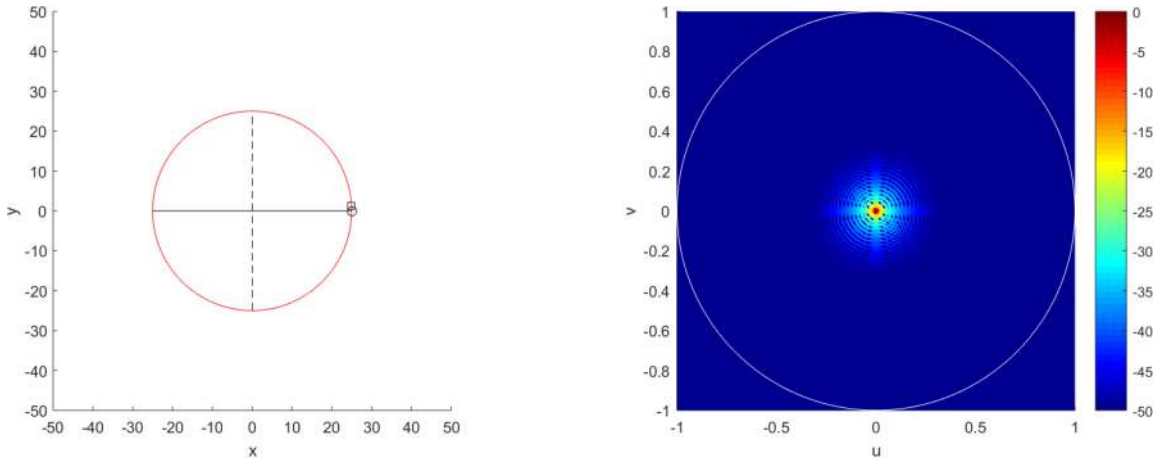

(a) Aperture geometry (in $[\lambda]$)

(b) $I(\boldsymbol{k})$ for uniform co-phasal illumination (FF [dB])

FIGURE 5. Circular aperture, $D_A = 50\lambda$.

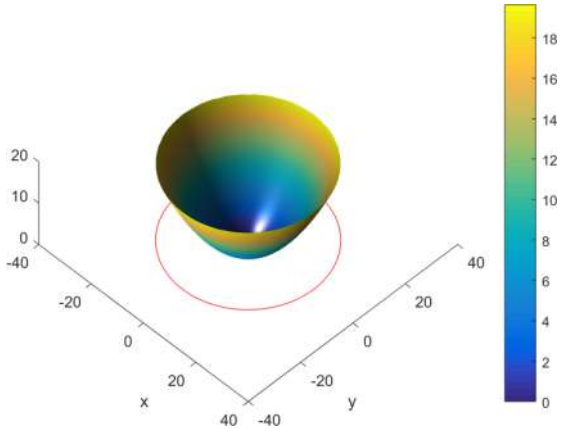

FIGURE 6. Circular Beam (Phase [rad]), $\lambda_1 = 1$, $\lambda_2 = 1$, $\theta = 0°$.

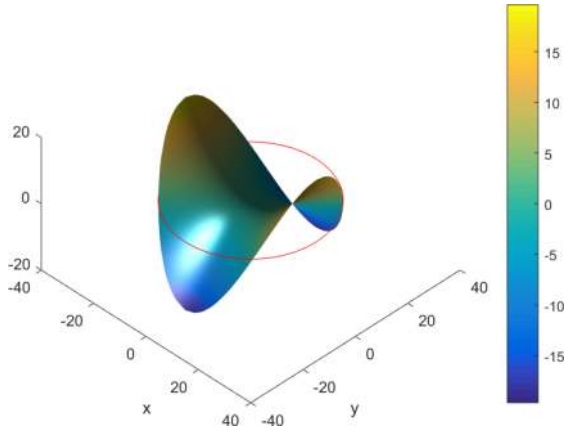

FIGURE 8. Circular Beam (Phase [rad]), $\lambda_1 = 1$, $\lambda_2 = -1$, $\theta = 0°$.

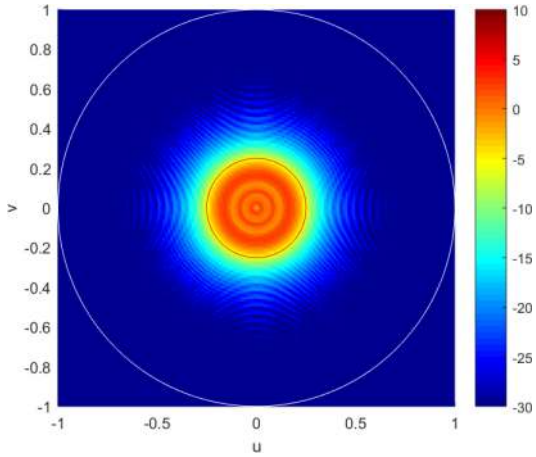

FIGURE 7. Circular Beam (FF [dB]), $\lambda_1 = 1$, $\lambda_2 = 1$, $\theta = 0°$.

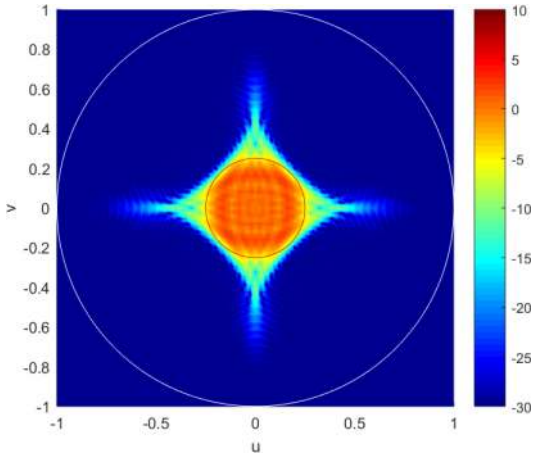

FIGURE 9. Circular Beam (FF [dB]), $\lambda_1 = 1$, $\lambda_2 = -1$, $\theta = 0°$.

phase approximation, is the genesis of our Monge–Ampère formulation.

We start focusing our attention on the problem of evaluating the asymptotic approximation of the radiation pattern $F(\boldsymbol{k})$ generated by an aperture distribution with real positive amplitude and phase $\phi(\boldsymbol{r})$ over the planar aperture domain $\boldsymbol{\Gamma}$.

The aim of the stationary phase method is to obtain an asymptotic approximation of $F(\boldsymbol{k})$ in the limit $\lambda \to 0$.

According to Watson [35], the principle of stationary phase was first used by Stokes [36] for the approximation of the Airy function and was later given its general formulation by Thompson [37] in his effort to describe the wave pattern behind a moving ship. The most general results and extensions are due to the work of van der Corput [38], [39], [40]. Erdelyi [41], [42], and de Bruijn [43] detailed this method in their books on asymptotic methods which become standard references. Considering that the integrand is bounded and rapidly oscillating, the main contributions will come from the critical points which correspond to a stationarity condition of the phase,

$$\nabla_{\boldsymbol{r}} \left(\phi(\boldsymbol{r}) - \boldsymbol{k} \cdot \boldsymbol{r}\right)|_{\boldsymbol{r}_s} = 0. \tag{4}$$

We can thus consider the observation point $\boldsymbol{k}$ determined by the stationarity condition $\boldsymbol{k}_s = \boldsymbol{k}_s(\boldsymbol{r}_s)$,

$$\boldsymbol{k}_s = \nabla\phi(\boldsymbol{r})|_{\boldsymbol{r}_s}. \tag{5}$$

Assuming that the amplitude $f(\boldsymbol{r})$ is slowly varying, we can Taylor expand the phase term $\phi(\boldsymbol{r})$ to the second order at $\boldsymbol{r}_s$,

$$\begin{aligned}\phi(\boldsymbol{r}) \approx \phi(\boldsymbol{r}_s) &+ (\boldsymbol{r} - \boldsymbol{r}_s)^T \nabla\phi(\boldsymbol{r})|_{\boldsymbol{r}_s} \\ &+ \frac{1}{2}(\boldsymbol{r} - \boldsymbol{r}_s)^T \mathbf{H}(\phi(\boldsymbol{r}))|_{\boldsymbol{r}_s}(\boldsymbol{r} - \boldsymbol{r}_s),\end{aligned} \tag{6}$$

where $\mathbf{H}$ is the Hessian operator (often indicated as D^2),

$$\begin{aligned}\mathbf{H}(\phi(\boldsymbol{r})) &= D^2(\phi(\boldsymbol{r})) \\ &= \mathbf{J}(\nabla\phi(\boldsymbol{r})),\end{aligned} \tag{7}$$

being J the Jacobian operator. The Hessian matrix $\mathbf{H}\phi|_{\boldsymbol{r}_s}$ is an important object in Geometric Optics (see, *e.g.,* [58] and the Appendix A for further comments). The Fourier integral evaluated in the corresponding direction $\boldsymbol{k}_s$ can be approximated as (refer to Appendix A for full details),

$$F(\boldsymbol{k}_s) \approx f|_{\boldsymbol{r}_s} e^{j\left(\phi|_{\boldsymbol{r}_s} - \boldsymbol{k}_s \cdot \boldsymbol{r}_s\right)} \frac{2\pi}{\sqrt{|\lambda_1 \lambda_2|}} e^{j\frac{\pi}{4}(\mathrm{sign}(\lambda_1) + \mathrm{sign}(\lambda_2))}, \tag{8}$$

where λ_1 and λ_2 are the real eigenvalues of the Hessian matrix $\mathbf{H}\phi|_{\boldsymbol{r}_s}$. Considering now the magnitude squared of both sides of (8) and the fact that the product of the eigenvalues of a matrix corresponds to its determinant,

$$\lambda_1 \lambda_2 = \det \mathbf{H}\phi|_{\boldsymbol{r}_s} \tag{9}$$

we obtain,

$$|F(\boldsymbol{k}_s)|^2 = \frac{(2\pi)^2}{\left|\det \mathbf{H}\phi|_{\boldsymbol{r}_s}\right|} f^2(\boldsymbol{r}_s)\ . \tag{10}$$

This equation can be further simplified assuming that, for the aperture variable $\boldsymbol{r}$, the stationarity condition (5) determines an observation direction $\nabla\phi(\boldsymbol{r})$, and rearranged as

$$|\det(\mathbf{H}\phi)| = (2\pi)^2 \frac{f^2(\boldsymbol{r})}{|F(\nabla\phi(\boldsymbol{r}))|^2} \tag{11}$$

which, remarkably, is a non-linear partial differential equation of the Monge-Ampère type that will be further discussed in next sections. It must be completed with the energy conservation condition of the Parseval–Plancherel theorem, which in $\mathbb{R}^2$ reads [34],

$$\iint_{\boldsymbol{\Gamma}} f^2(\boldsymbol{r}) d\boldsymbol{r} = \frac{1}{(2\pi)^2} \iint_{\mathbb{R}^2} |F(\boldsymbol{k})|^2 d\boldsymbol{k}, \tag{12}$$

with the magnitude square at the left hand side absorbed by the assumption on real positiveness of $f(\boldsymbol{r})$, and the integration domain limited to the aperture $\boldsymbol{\Gamma}$ where $f(\boldsymbol{r}) \neq 0$.

III. THE EQUIVALENT MONGE-AMPÈRE PDE FOR THE INTENSITIES

Introducing the intensity of the aperture field, $i(\boldsymbol{r})$, and of the pattern, $I(\boldsymbol{k})$, respectively,

$$i(\boldsymbol{r}) = |f(\boldsymbol{r})|^2 \tag{13}$$

$$I(\boldsymbol{k}) = \frac{1}{(2\pi)^2}|F(\boldsymbol{k})|^2, \tag{14}$$

we can reduce the Monge-Ampère PDE on the squared fields magnitudes (11) to a more insightful Monge-Ampère PDE on the intensities,

$$|\det(\mathbf{H}\phi)| = \frac{i(\boldsymbol{r})}{I(\nabla\phi(\boldsymbol{r}))}. \tag{15}$$

The Parseval–Plancherel energy conservation condition (12) becomes,

$$\iint_{\boldsymbol{\Gamma}} i(\boldsymbol{r}) d\boldsymbol{r} = \iint_{\mathbb{R}^2} I(\boldsymbol{k}) d\boldsymbol{k}. \tag{16}$$

The partial differential equation derived by the stationary phase method (15), together with the energy conservation normalization (16) can now be used in a constructive way to state the asymptotic phase-only synthesis problem.

Asymptotic Synthesis Problem - Given an aperture distribution with intensity $i(\boldsymbol{r})$ over a planar aperture domain $\boldsymbol{\Gamma}$, and assigned a desired pattern intensity $I_d(\boldsymbol{k})$ in the main beam domain $\boldsymbol{\Omega}$, both normalized such that,

$$\iint_{\boldsymbol{\Gamma}} i(\boldsymbol{r}) d\boldsymbol{r} = \iint_{\boldsymbol{\Omega}} I_d(\boldsymbol{k}) d\boldsymbol{k} = 1, \tag{17}$$

where $\boldsymbol{\Gamma}$ and $\boldsymbol{\Omega}$ are bounded sets in $\mathbb{R}^2$, find the phase function $\phi(\boldsymbol{r})$ over $\boldsymbol{\Gamma}$ such that

$$\nabla\phi \colon \boldsymbol{\Gamma} \to \boldsymbol{\Omega} \tag{18}$$

and the following Monge-Ampère PDE is satisfied,

$$|\det(\mathbf{H}\phi)| = \frac{i(\boldsymbol{r})}{I_d(\nabla\phi(\boldsymbol{r}))} \tag{19}$$

The Monge-Ampère equation has, in $\mathbb{R}^2$, the general form [48], [49], [50], [51],

$$\det(\mathbf{H}\phi) = \Psi(\boldsymbol{r}, \phi, \nabla\phi), \quad \boldsymbol{r} \in \boldsymbol{\Gamma} \subseteq \mathbb{R}^2 \tag{20}$$

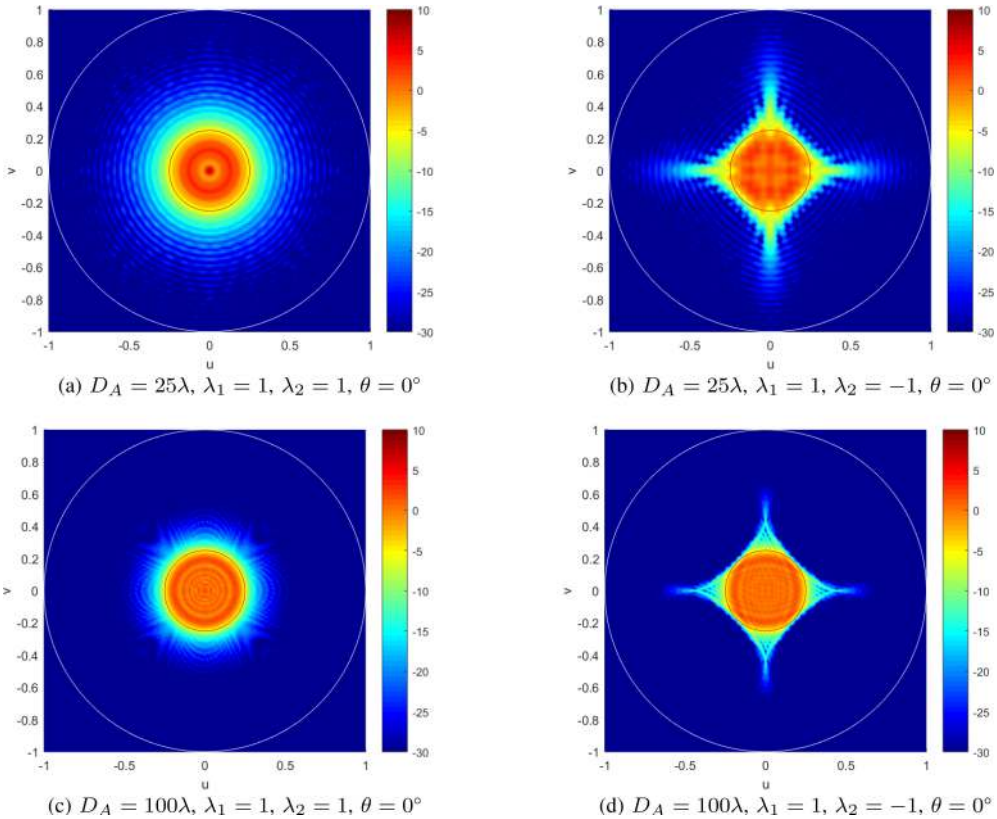

(a) $D_A = 25\lambda,\ \lambda_1 = 1,\ \lambda_2 = 1,\ \theta = 0°$ (b) $D_A = 25\lambda,\ \lambda_1 = 1,\ \lambda_2 = -1,\ \theta = 0°$

(c) $D_A = 100\lambda,\ \lambda_1 = 1,\ \lambda_2 = 1,\ \theta = 0°$ (d) $D_A = 100\lambda,\ \lambda_1 = 1,\ \lambda_2 = -1,\ \theta = 0°$

FIGURE 10. Circular Aperture/Beam - Asymptotic Behaviour, $u_0 = .25$ (FF [dB]).

It is categorised as a "fully" nonlinear partial differential equation due to the appearance of a non-linearity for the highest order derivatives of the unknown function $\phi(\boldsymbol{r})$. Indeed the explicit expression of the Hessian determinant is,

$$\det(\mathbf{H}\phi) = \det\begin{bmatrix} \dfrac{\partial^2\phi}{\partial x^2} & \dfrac{\partial^2\phi}{\partial x\partial y} \\ \dfrac{\partial^2\phi}{\partial y\partial x} & \dfrac{\partial^2\phi}{\partial y^2} \end{bmatrix} = \frac{\partial^2\phi}{\partial x^2}\frac{\partial^2\phi}{\partial y^2} - \left(\frac{\partial^2\phi}{\partial y\partial x}\right)^2 \tag{21}$$

In its historical appearance, the Monge–Ampère PDE was first introduced by Monge [48] and later by Ampère [49] to address the problem of determining a surface with prescribed Gaussian curvature. The link between the Monge–Ampère PDE and the "Optimal Mass Transport" problem, first formulated by Monge [56], has been explored from several perspectives. In a companion paper [57] this link will be exploited to solve the most general form of the asymptotic phase synthesis problem. Nonetheless, considering that some additional restrictions will need to be applied (e.g., convexity of $\phi(\boldsymbol{r})$), it will be useful to first interpret the problem at hand as transport map problem which admits a broader class of solutions and will also allow to derive analytical solutions for specific cases.

The boundary condition (18) is the so-called "second boundary value condition", and it is required in the Monge formulation of the Optimal Transport problem [52], [53]. The condition requires that the domain $\boldsymbol{\Gamma} \subseteq \mathbb{R}^2$ is fully mapped through the gradient of $\phi(\boldsymbol{r})$ to the domain $\boldsymbol{\Omega} \subseteq \mathbb{R}^2$.

IV. THE EQUIVALENT IRROTATIONAL TRANSPORT MAP PROBLEM

Expressing the Hessian matrix as the Jacobian of the gradient (7), $\mathbf{H}\phi = \mathbf{J}(\nabla\boldsymbol{\phi})$, we can lower the order of the Monge-Ampère PDE obtaining an equivalent problem on $\nabla\phi(\boldsymbol{r})$ rather than on $\phi(\boldsymbol{r})$. Considering the role of the stationary condition to map a point in $\boldsymbol{r}$ to one in $\boldsymbol{k}$, we essentially seek for a mapping function $\boldsymbol{k} = \boldsymbol{T}(\boldsymbol{r})$. A good candidate for the mapping would be a bijective[2] vectorial function $\boldsymbol{T} : \boldsymbol{\Gamma} \to \boldsymbol{\Omega}$. Thus the problem can be reformulated in $\boldsymbol{T}$ as follows:

Equivalent Irrotational Transport Map Problem - Assigned the positive intensities $i(\boldsymbol{r})$, $\boldsymbol{r} \in \boldsymbol{\Gamma}$, and $I_d(\boldsymbol{k})$, $\boldsymbol{k} \in \boldsymbol{\Omega}$, normalized according to (16), find the bijective transport map $\boldsymbol{T} : \boldsymbol{\Gamma} \to \boldsymbol{\Omega}$ satisfying:

$$|\det(\mathbf{J}\boldsymbol{T})| = \frac{i(\boldsymbol{r})}{I_d(\boldsymbol{T}(\boldsymbol{r}))} \tag{22}$$

such that the transport map $\boldsymbol{T}$ is irrotational,

$$\boldsymbol{T}(\boldsymbol{r}) = \nabla\phi(\boldsymbol{r}) \tag{23}$$

[2]i.e., an injective (one-to-one) and surjective (onto) mapping.

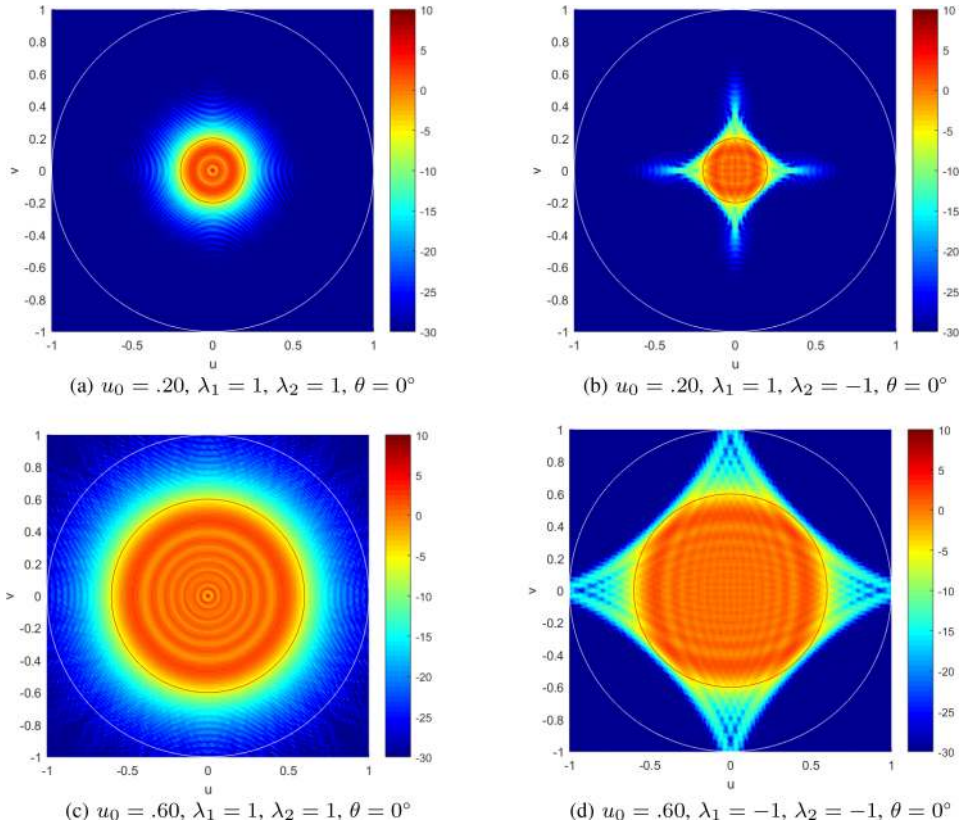

FIGURE 11. Circular Aperture/Beam - Beam Zooming Behaviour, $D_A = 50\lambda$ (FF [dB]).

The transport map $\boldsymbol{k} = \boldsymbol{T}(\boldsymbol{r})$ must preserve the transported quantity in the transport $\boldsymbol{r} \to \boldsymbol{k}$. To understand the mathematical implications we can observe that an infinitesimal volume in $\boldsymbol{r}$ would be defined by the differential $i(\boldsymbol{r})d\boldsymbol{r}$. Similarly an infinitesimal volume in $\boldsymbol{k}$ would be defined by $I_d(\boldsymbol{k})d\boldsymbol{k}$. The transported quantity will be preserved if,

$$i(\boldsymbol{r})d\boldsymbol{r} = I_d(\boldsymbol{T}(\boldsymbol{r}))d\boldsymbol{k} \tag{24}$$

Using the Jacobian determinant for the change of variables, $d\boldsymbol{k} = \det(\boldsymbol{JT})d\boldsymbol{r}$, we obtain,

$$i(\boldsymbol{r})d\boldsymbol{r} = I_d(\boldsymbol{T}(\boldsymbol{r}))\det(\boldsymbol{JT})d\boldsymbol{r} \tag{25}$$

which, apart the possible change of sign of the determinant, corresponds to the PDE (22).

In the area of pure mathematics that is called measure theory, where the intensities correspond to probability densities, a valid transport map is said to "push-forward" the measure $i(\boldsymbol{r})d\boldsymbol{r}$ onto $I_d(\boldsymbol{k})d\boldsymbol{k}$, if for all bounded sets $\boldsymbol{\Omega}' \subseteq \boldsymbol{\Omega}$,

$$\iint_{\boldsymbol{T}^{-1}(\boldsymbol{\Omega})} i(\boldsymbol{r})d\boldsymbol{r} = \iint_{\boldsymbol{\Omega}'} I_d(\boldsymbol{k})d\boldsymbol{k}, \quad \boldsymbol{\Gamma}' = \boldsymbol{T}^{-1}(\boldsymbol{\Omega}') \subseteq \boldsymbol{\Gamma} \tag{26}$$

Differential (25) and integral (26) "measure preserving" conditions are equivalent; a transport map $\boldsymbol{T} : \boldsymbol{\Gamma} \to \boldsymbol{\Omega}$ fulfilling them is denoted as push-forward,

$$\boldsymbol{T}_{\#} i = I_d \tag{27}$$

Making explicit the vector components of the mapping,

$$\boldsymbol{T} = \begin{bmatrix} T_x \\ T_y \end{bmatrix}, \tag{28}$$

the explicit expression for the Jacobian determinant is,

$$\det(\boldsymbol{JT}) = \det\begin{bmatrix} \dfrac{\partial T_x}{\partial x} & \dfrac{\partial T_x}{\partial y} \\ \dfrac{\partial T_y}{\partial x} & \dfrac{\partial T_y}{\partial y} \end{bmatrix} = \\ = \frac{\partial T_x}{\partial x}\frac{\partial T_y}{\partial y} - \frac{\partial T_x}{\partial y}\frac{\partial T_y}{\partial x}. \tag{29}$$

The transport equation (22) identifies a set of transport maps $\Pi(i, I_d)$ that push forward i in I_d (where the domains $\boldsymbol{\Gamma}$ and $\boldsymbol{\Omega}$ are implicit). Within this set, irrotational transport maps (23), can be integrated to obtain a solution to the Monge-Ampère PDE (19) and (18). The necessary condition for the map $\boldsymbol{T}$ to be irrotational is the symmetry of the Jacobian (see, for example [59, Th. 10.6]),

$$\frac{\partial T_x}{\partial y} = \frac{\partial T_y}{\partial x}. \tag{30}$$

which corresponds to the interchangeability of the order of differentiation for the mixed partial derivatives of $\phi(\boldsymbol{r})$,

$$\frac{\partial^2 \phi}{\partial x \partial y} = \frac{\partial^2 \phi}{\partial y \partial x}. \tag{31}$$

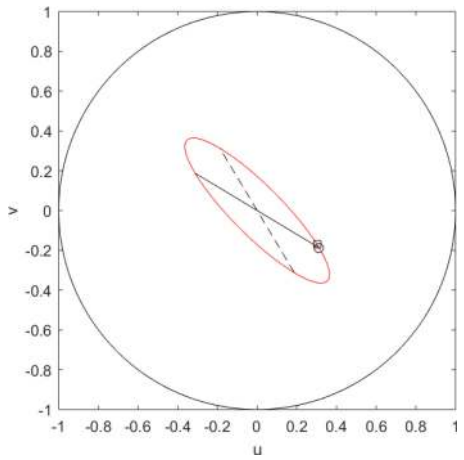

FIGURE 12. Elliptical Beam (Map), $\lambda_1 = 0.5$, $\lambda_2 = 2$, $\theta = 45°$.

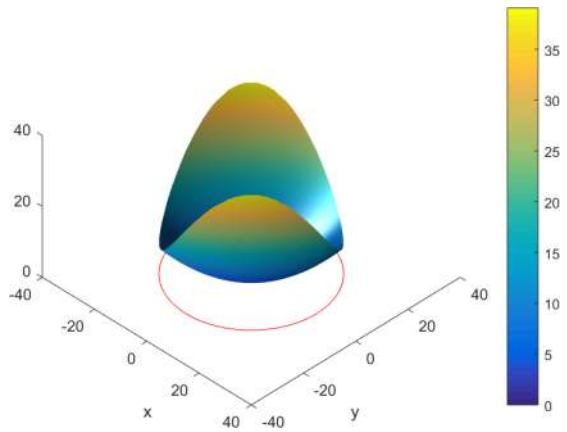

FIGURE 13. Elliptical Beam (Phase [rad]), $\lambda_1 = 0.5$, $\lambda_2 = 2$, $\theta = 45°$.

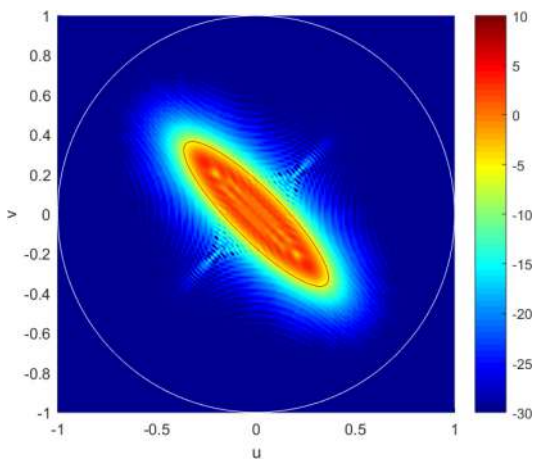

FIGURE 14. Elliptical Beam (FF [dB]), $\lambda_1 = 0.5$, $\lambda_2 = 2$, $\theta = 45°$.

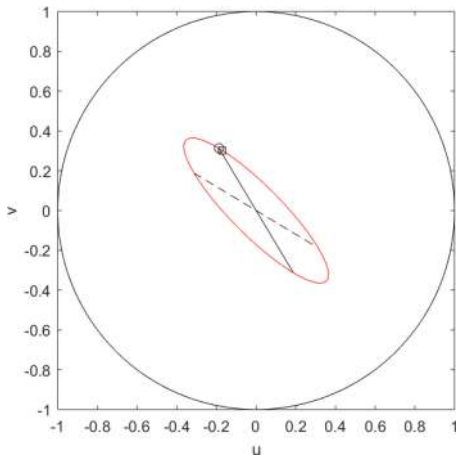

FIGURE 15. Elliptical Beam (Map), $\lambda_1 = 0.5$, $\lambda_2 = -2$, $\theta = 45°$.

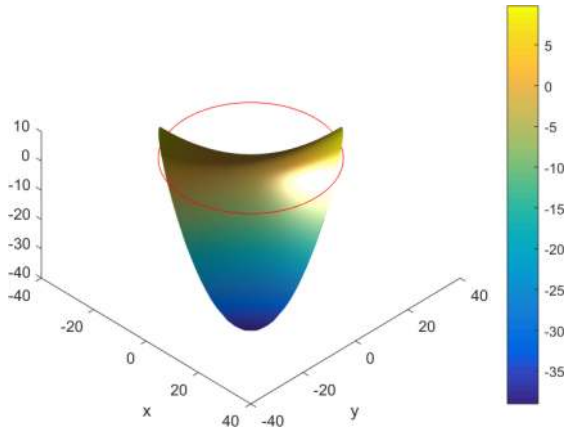

FIGURE 16. Elliptical Beam (Phase [rad]), $\lambda_1 = 0.5$, $\lambda_2 = -2$, $\theta = 45°$.

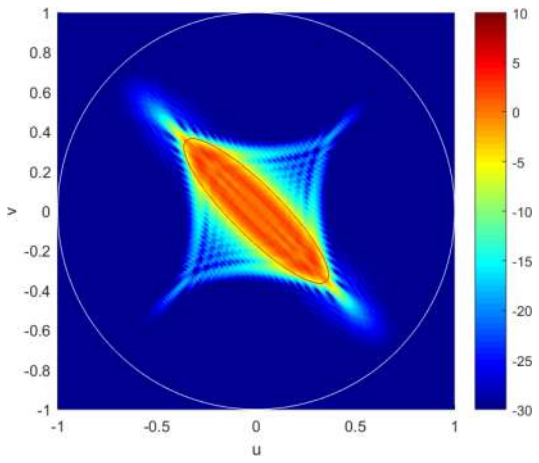

FIGURE 17. Elliptical Beam (FF [dB]), $\lambda_1 = 0.5$, $\lambda_2 = -2$, $\theta = 45°$.

Condition (30) becomes also sufficient if it is satisfied on an open convex set (see, for example [59, Th. 10.9]).

A simple class of transport maps that can find direct application to our phase synthesis problem is the class of linear transforms. A linear map has the general form of an "affine" transformation,

$$\boldsymbol{T}(\boldsymbol{r}) = \mathbf{A}\boldsymbol{r} + \mathbf{t}_0 \tag{32}$$

where $\mathbf{A}$ is a (2×2) matrix,

$$\mathbf{A} = \begin{bmatrix} a & b \\ c & d \end{bmatrix}, \qquad \mathbf{t}_0 = \begin{bmatrix} t_{0x} \\ t_{0y} \end{bmatrix} \tag{33}$$

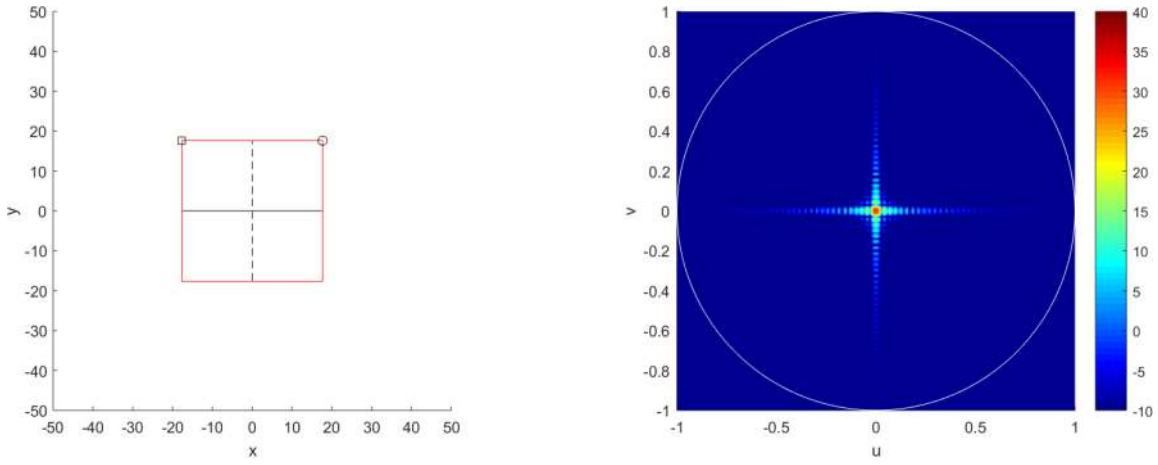

(a) Square Aperture geometry (in $[\lambda]$)

(b) $I(\boldsymbol{k})$ for uniform co-phasal illumination (FF [dB])

FIGURE 18. Square aperture, $D_A = 50\lambda$.

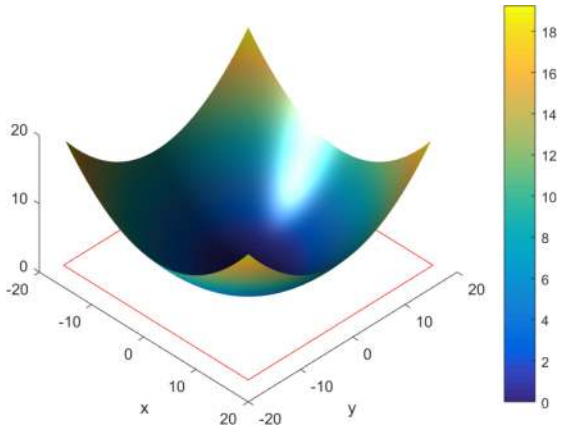

FIGURE 19. Square Beam (Phase [rad]), $\lambda_1 = 1$, $\lambda_2 = 1$, $\theta = 0°$.

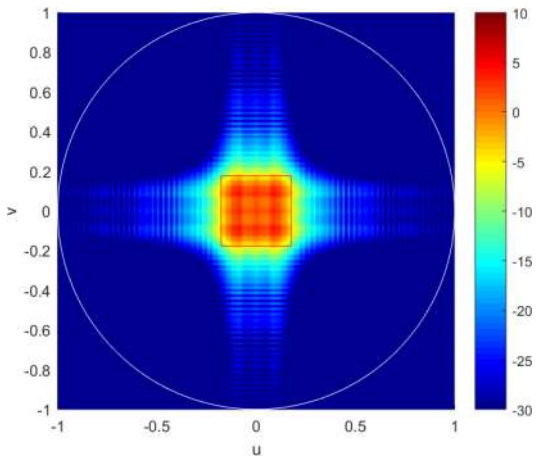

FIGURE 20. Square Beam (FF [dB]), $\lambda_1 = 1$, $\lambda_2 = 1$, $\theta = 0°$.

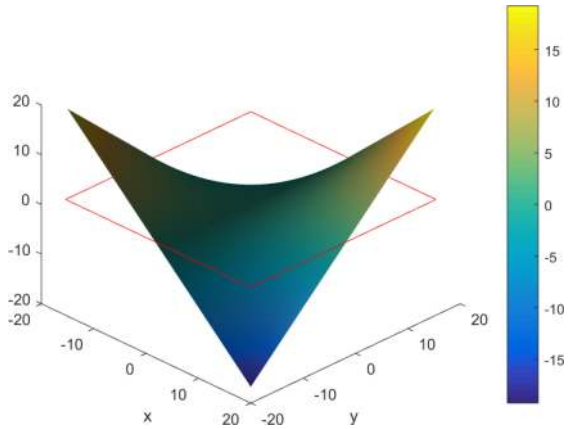

FIGURE 21. Square Beam (Phase [rad]), $\lambda_1 = 1$, $\lambda_2 = -1$, $\theta = 45°$.

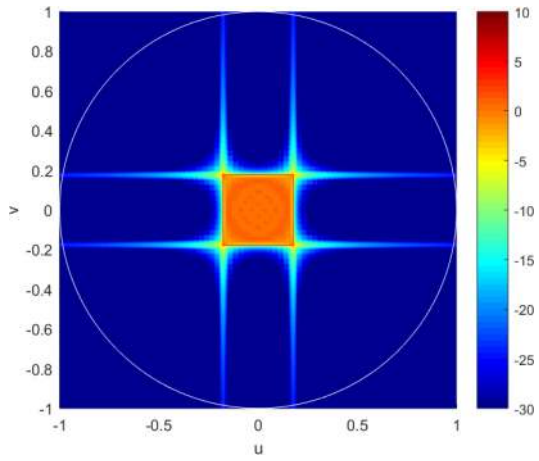

FIGURE 22. Square Beam (FF [dB]), $\lambda_1 = 1$, $\lambda_2 = -1$, $\theta = 45°$.

with determinant, $A \triangleq \det \mathbf{A} = ab - cd$. The matrix $\mathbf{A}$ also corresponds to the Jacobian of the map (32), $\boldsymbol{J}\mathbf{T} = \mathbf{A}$, and A to the Jacobian determinant, $\det(\boldsymbol{J}\mathbf{T}) = A$.

Assigned $i(\boldsymbol{r})$ on $\boldsymbol{\Gamma}$, the affine transformation (32) is a suitable transport map for $I_d(\boldsymbol{k})$ on $\boldsymbol{\Omega}$ if the following two conditions are satisfied:

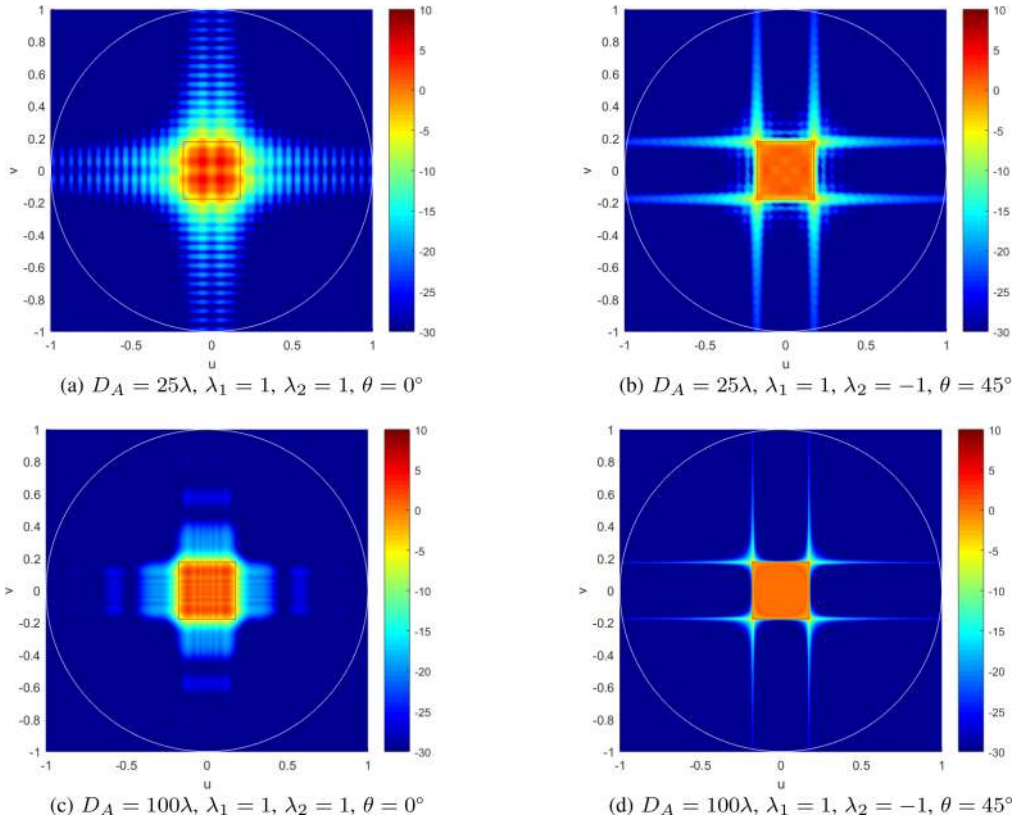

(a) $D_A = 25\lambda$, $\lambda_1 = 1$, $\lambda_2 = 1$, $\theta = 0°$ (b) $D_A = 25\lambda$, $\lambda_1 = 1$, $\lambda_2 = -1$, $\theta = 45°$

(c) $D_A = 100\lambda$, $\lambda_1 = 1$, $\lambda_2 = 1$, $\theta = 0°$ (d) $D_A = 100\lambda$, $\lambda_1 = 1$, $\lambda_2 = -1$, $\theta = 45°$

FIGURE 23. Square Aperture/Beam - Asymptotic Behaviour, $u_0 = .25$ (FF [dB]).

$$I_d(\mathbf{A}\boldsymbol{r} + \mathbf{t}_0) = \frac{1}{|A|} i(\boldsymbol{r}) \tag{34}$$

$$\boldsymbol{\Omega} = \mathbf{A}\boldsymbol{\Gamma} + \mathbf{t}_0 \tag{35}$$

Equation (34) allows to satisfy the differential transport condition (22); and (35) the domain mapping condition. For this second condition it can be observed that an affine transformation $\mathbf{A}\boldsymbol{r}$ maps a domain $\boldsymbol{\Gamma}$ in $\mathbf{A}\boldsymbol{\Gamma} + \mathbf{t}_0$. The vector $\mathbf{t}_0$ is constant and acts as a rigid translation.

We can now enforce the necessary condition on the transport map to be irrotational (30), which translates in the symmetry, $c = b$, of the Jacobian matrix $\mathbf{A}$,

$$\mathbf{A} = \mathbf{S} = \mathbf{S}^T, \qquad \mathbf{S} = \begin{bmatrix} a & b \\ b & d \end{bmatrix} \tag{36}$$

Using the decomposition (57) of real symmetric matrices described in Appendix B,

$$\mathbf{S} = \mathbf{R}(\theta) \begin{bmatrix} \text{sign}(\lambda_1) & 0 \\ 0 & \text{sign}(\lambda_2) \end{bmatrix} \begin{bmatrix} |\lambda_1| & 0 \\ 0 & |\lambda_2| \end{bmatrix} \mathbf{R}(-\theta) \tag{37}$$

we can interpret the symmetric affine transformation as a dilation (contraction) of a factor $|\lambda_1|$ along the axis of angle θ, and a dilation (contraction) of a factor $|\lambda_2|$ along the orthogonal axis. The factor $|S| = |\lambda_1||\lambda_2| = \det(\mathbf{S})$ is a global scale parameter that defines the area expansion (compression); if $|S| = 1$ the transform is said to be "equiareal". The negative sign of one of the eigenvalues determines a reflection along the relevant axis. If both the eigenvalues are negative the transform is said to be a "point reflection" and corresponds to an 180 degrees rotation.

Neglecting the constant translation vector $\mathbf{t}_0$, the transformation of the vertices of a unit square offers an insightful visualization of the effects of the symmetric affine transform $\mathbf{S}\boldsymbol{r}$.

$$\begin{bmatrix} 0 \\ 0 \end{bmatrix} \to \begin{bmatrix} 0 \\ 0 \end{bmatrix} \qquad \begin{bmatrix} 1 \\ 0 \end{bmatrix} \to \begin{bmatrix} a \\ b \end{bmatrix}$$

$$\begin{bmatrix} 0 \\ 1 \end{bmatrix} \to \begin{bmatrix} b \\ d \end{bmatrix} \qquad \begin{bmatrix} 1 \\ 1 \end{bmatrix} \to \begin{bmatrix} a+b \\ b+d \end{bmatrix}$$

The transformed parallelogram (affine transformations preserve parallel lines) is shown in Fig. 4.

Assuming that the assigned intensities admit a linear irrotational transport map $\boldsymbol{T}(\boldsymbol{r}) = \mathbf{S}\boldsymbol{r} + \mathbf{t}_0$, with $\mathbf{S}$ symmetric, to solve the Monge-Ampère PDE we need to find the "primitive function" $\phi(\boldsymbol{r})$ whose gradient is the transport map $\boldsymbol{T}(\boldsymbol{r})$ (23). Neglecting an unmeaningful constant we can verify that the quadratic form,

$$\phi(\boldsymbol{r}) = \frac{1}{2} \boldsymbol{r}^T (\mathbf{S} + \mathbf{Q}) \boldsymbol{r} + \boldsymbol{r}^T \mathbf{t}_0 \tag{38}$$

with $\mathbf{S}$ real symmetric (36), and $\mathbf{Q}$ real antisymmetric,

$$\mathbf{Q} = -\mathbf{Q}^T, \qquad \mathbf{Q} = \begin{bmatrix} 0 & -c \\ c & 0 \end{bmatrix} \tag{39}$$

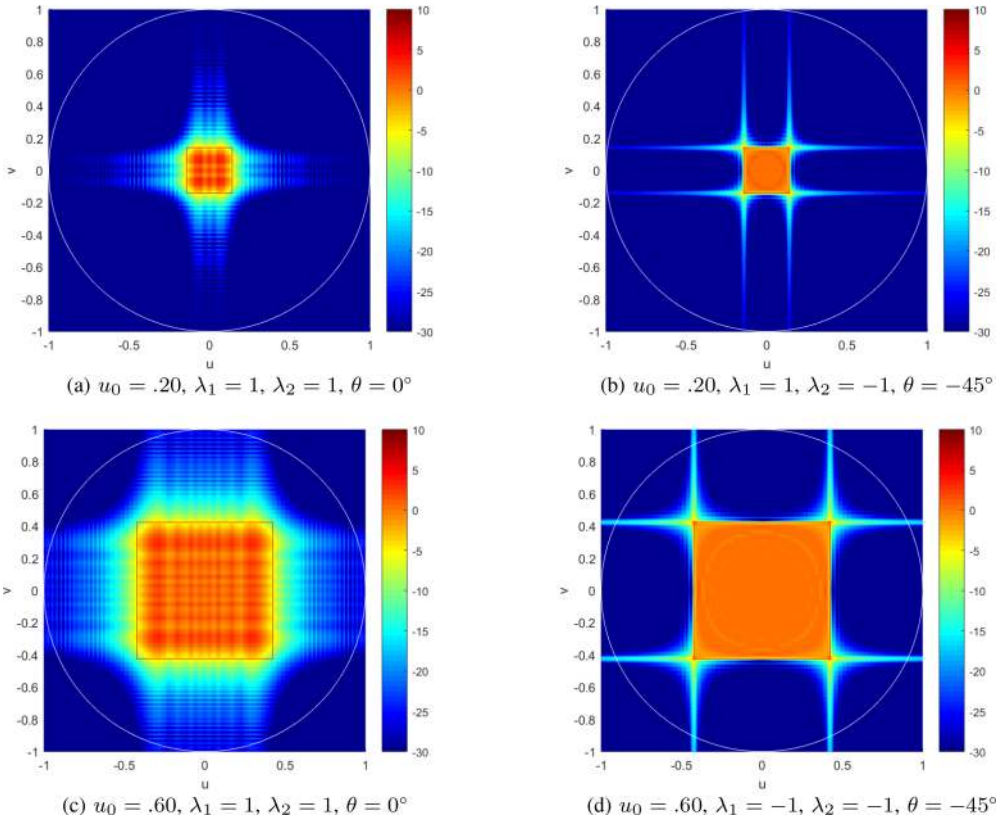

(a) $u_0 = .20,\ \lambda_1 = 1,\ \lambda_2 = 1,\ \theta = 0°$ (b) $u_0 = .20,\ \lambda_1 = 1,\ \lambda_2 = -1,\ \theta = -45°$

(c) $u_0 = .60,\ \lambda_1 = 1,\ \lambda_2 = 1,\ \theta = 0°$ (d) $u_0 = .60,\ \lambda_1 = -1,\ \lambda_2 = -1,\ \theta = -45°$

FIGURE 24. Square Aperture/Beam - Beam Zooming Behaviour, $D_A = 50\lambda$ (FF [dB]).

has the gradient,

$$\nabla\phi(\boldsymbol{r}) = \frac{1}{2}\Big[(\mathbf{S}+\mathbf{Q}) + (\mathbf{S}+\mathbf{Q})^T\Big]\boldsymbol{r} + \mathbf{t}_0 = \mathbf{S}\boldsymbol{r} + \mathbf{t}_0\ , \tag{40}$$

which is the sought linear irrotational transport map. The matrix $\mathbf{Q}$ is irrelevant in terms of fulfillment of the transport conditions and is assumed to be null, $\mathbf{Q} = 0$.

V. IRROTATIONAL LINEAR TRANSPORT MAP: RESULTS

In the following sub-sections we report results of asymptotic phase only syntheses based on irrotational transport maps of the form, $\boldsymbol{T}(\boldsymbol{r}) = \mathbf{S}\boldsymbol{r}$, with $\mathbf{S}$ real symmetric, providing a quadratic phase,

$$\phi(\boldsymbol{r}) = \frac{1}{2}\boldsymbol{r}^T\mathbf{S}\boldsymbol{r} \tag{41}$$

The analyses are performed on uniform antenna apertures $i(\boldsymbol{r}) = 1$ varying some of the parameters defining either the aperture or the affine transformation. In particular, the sensitivity to the following parameters has been explored and is reported below:

- Aperture rims (i.e., circle, square, triangle, rose);
- Aperture diameter, D_A (encircling diameter);
- Beam radius, u_0 (beam encircling radius before dilation/contraction);
- Axes reflection, sign($\lambda_{1,2}$);
- Axes rotation angle, θ;
- Axes dilation/contraction, $|\lambda_{1,2}|$;

For convenience, the real symmetric matrix $\mathbf{S}$ representing the affine transformation is represented as the product of a scale parameter, s_0, which allows to match the aperture encircling diameter (D_A) to beam encircling radius (u_0), times a "equiareal" affine transformation of the form (37),

$$\mathbf{S} = s_0\ \mathbf{R}(\theta)\begin{bmatrix}\text{sign}(\lambda_1) & 0\\ 0 & \text{sign}(\lambda_2)\end{bmatrix}\begin{bmatrix}|\lambda_1| & 0\\ 0 & |\lambda_2|\end{bmatrix}\mathbf{R}(-\theta) \tag{42}$$

This corresponds to the composition of a first counter-clockwise rotation ($\mathbf{R}(-\theta)$), a dilation/compression ($|\lambda_{1,2}|$) and reflection (for negative sign($\lambda_{1,2}$)) along the principal axis, a second clockwise rotation ($\mathbf{R}(\theta)$), and a final homogeneous dilation (s_0) along both axis.

The decomposition (42) allows highlighting that, while a simple rotation is not admissible due to the lack of symmetry of the matrix $\mathbf{R}(\theta)$, a rotation of the target beam is achievable if one of the axis is reflected (with $\lambda_1 = -\lambda_2$)). In this case we can write,

$$\mathbf{R}(\theta)\begin{bmatrix}1 & 0\\ 0 & -1\end{bmatrix}\mathbf{R}(-\theta) = \mathbf{R}(2\theta)\begin{bmatrix}1 & 0\\ 0 & -1\end{bmatrix}, \tag{43}$$

which corresponds to the composition of a reflection along the y-axis and a rotation $\mathbf{R}(2\theta)$. The possibility of obtaining a beam shape corresponding to a rotated version of the reflected aperture shape is, to the best knowledge of the authors, reported here for the first time.

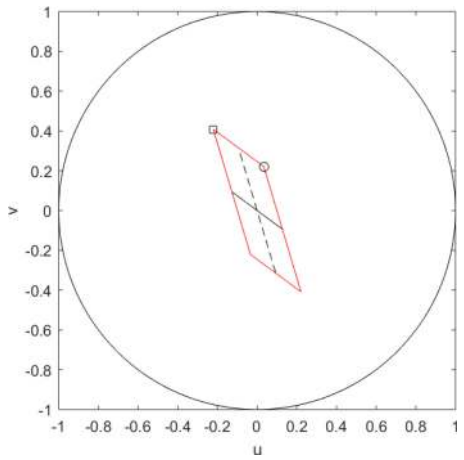

FIGURE 25. Deformed Square Beam (Map), $\lambda_1 = 0.5$, $\lambda_2 = 2$, $\theta = 22.25°$.

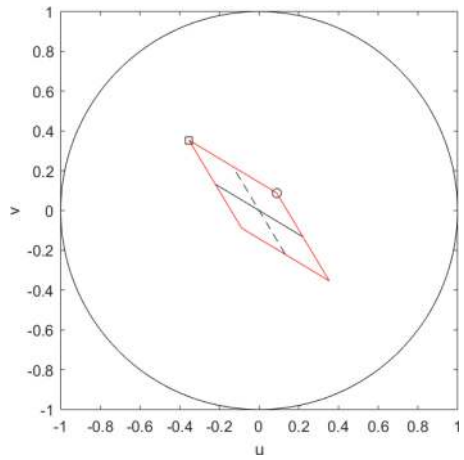

FIGURE 28. Deformed Square Beam (Map), $\lambda_1 = 0.5$, $\lambda_2 = 2$, $\theta = 45°$.

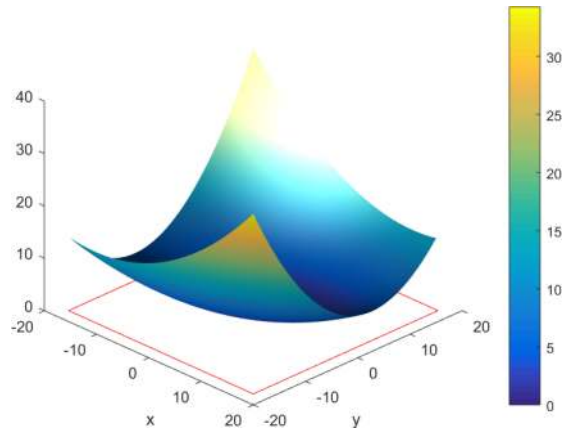

FIGURE 26. Deformed Square Beam (Phase [rad]), $\lambda_1 = 0.5$, $\lambda_2 = 2$, $\theta = 22.25°$e.

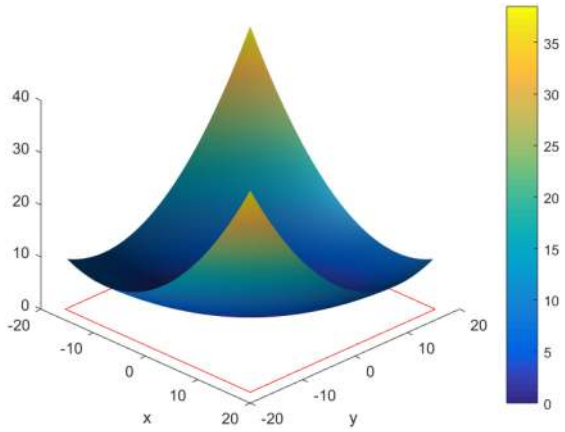

FIGURE 29. Deformed Square Beam (Phase [rad]), $\lambda_1 = 0.5$, $\lambda_2 = 2$, $\theta = 45°$.

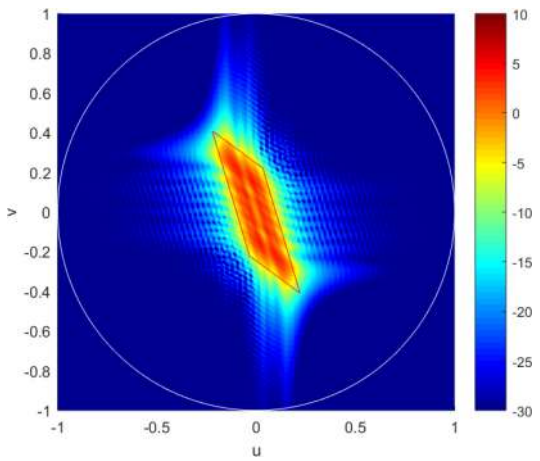

FIGURE 27. Deformed Square Beam (FF [dB]), $\lambda_1 = 0.5$, $\lambda_2 = 2$, $\theta = 22.25°$.

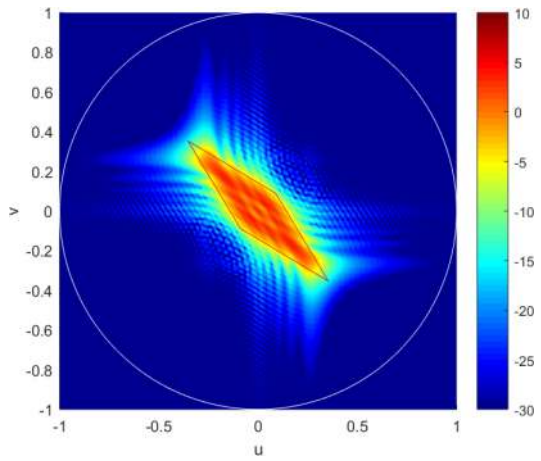

FIGURE 30. Deformed Square Beam (FF [dB]), $\lambda_1 = 0.5$, $\lambda_2 = 2$, $\theta = 45°$.

In the following subsections we analyse the results of the application of irrotational linear transport maps to different apertures and with different parameters of the mapping.

Please note that the radiation pattern intensities are reported in decibels [dBs]. They are normalized (in linear scale) to the average pattern intensity $I(\boldsymbol{k})$ in the main beam domain $\boldsymbol{\Omega}$ (red contour line). In these plots, the white circle will represent the visibility contour ($\sqrt{u^2 + v^2} = 1$).

A. CIRCULAR APERTURE

As first set of examples we report the results related to circular apertures. The far-field of a uniformly illuminated

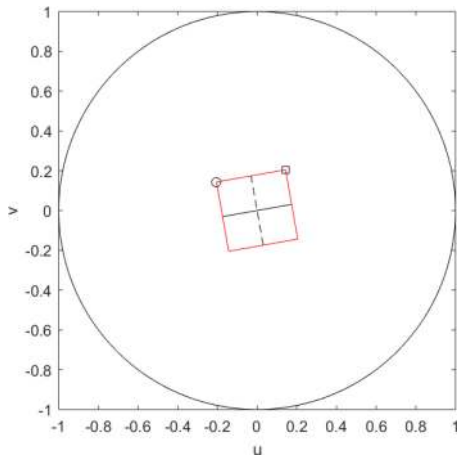

FIGURE 31. Rotated Square Beam (Map), $\lambda_1 = 1, \lambda_2 = -1, \theta = 95°$.

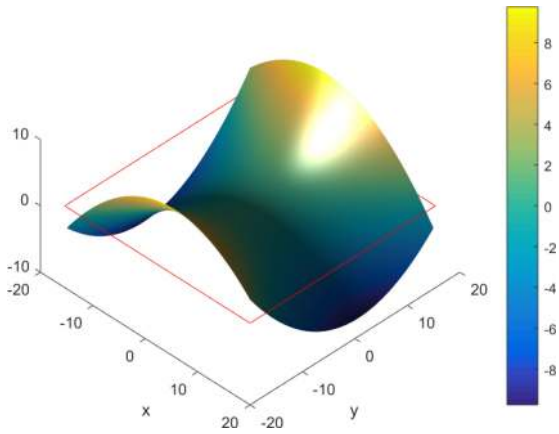

FIGURE 32. Rotated Square Beam (Phase [rad]), $\lambda_1 = 1, \lambda_2 = -1, \theta = 95°$.

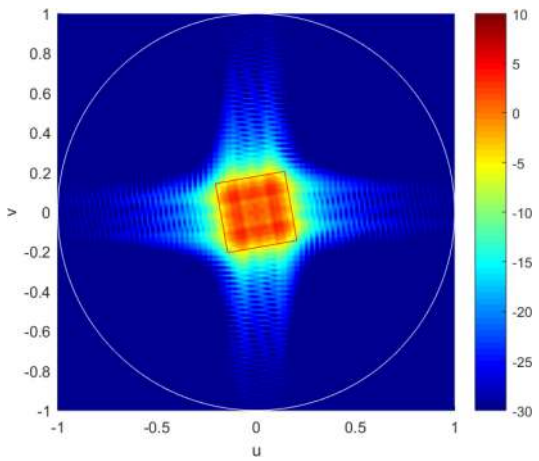

FIGURE 33. Rotated Square Beam (FF [dB]), $\lambda_1 = 1, \lambda_2 = -1, \theta = 95°$.

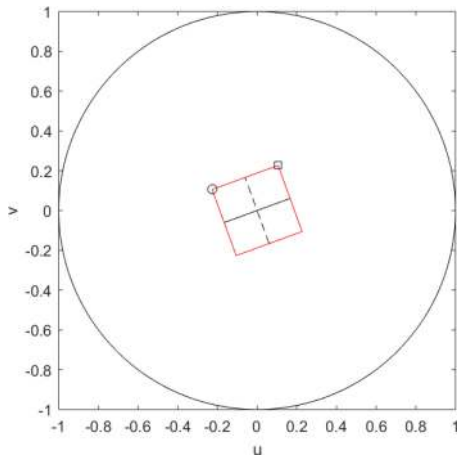

FIGURE 34. Rotated Square Beam (Map), $\lambda_1 = 1, \lambda_2 = -1, \theta = 100°$.

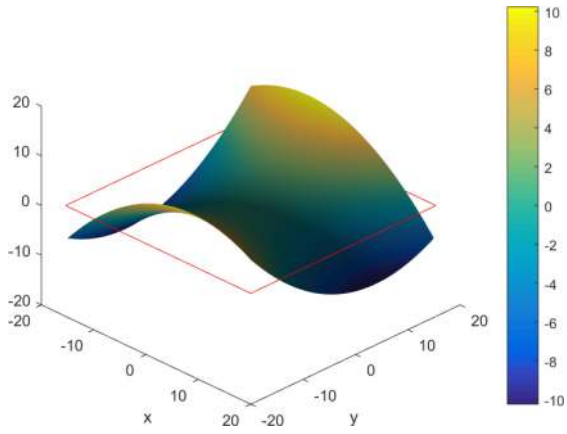

FIGURE 35. Rotated Square Beam (Phase [rad]), $\lambda_1 = 1, \lambda_2 = -1, \theta = 100°$.

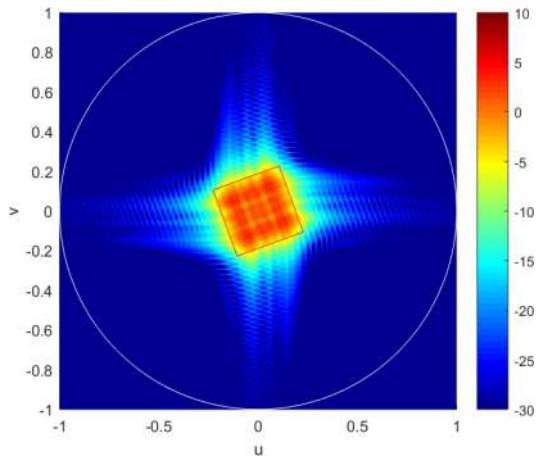

FIGURE 36. Rotated Square Beam (FF [dB]), $\lambda_1 = 1, \lambda_2 = -1, \theta = 100°$.

circular aperture of 50λ diameter (Fig. 5(a)) is shown in Fig. 5(b). The objective of the phase synthesis is to obtain a much broader circular beam of encircling radius $u_0 = 0.25$. Two alternative solutions correspond to selecting either concordant or discordant signs of $\lambda_{1,2}$ with non-dilated axes ($|\lambda_{1,2}| = 1$). The paraboloidal phase corresponding to concordant signs is shown in Fig. 6, and the relevant far field in Fig. 7. Similarly, for discordant signs (and non-dilated axes) the hyperbolic paraboloidal phase is shown in Fig. 8, and far field in Fig. 9. It can be well appreciated that the diffraction limited pattern of Fig. 5(b) is broadened to the match the desired circular beam of Fig. 7 and 9.

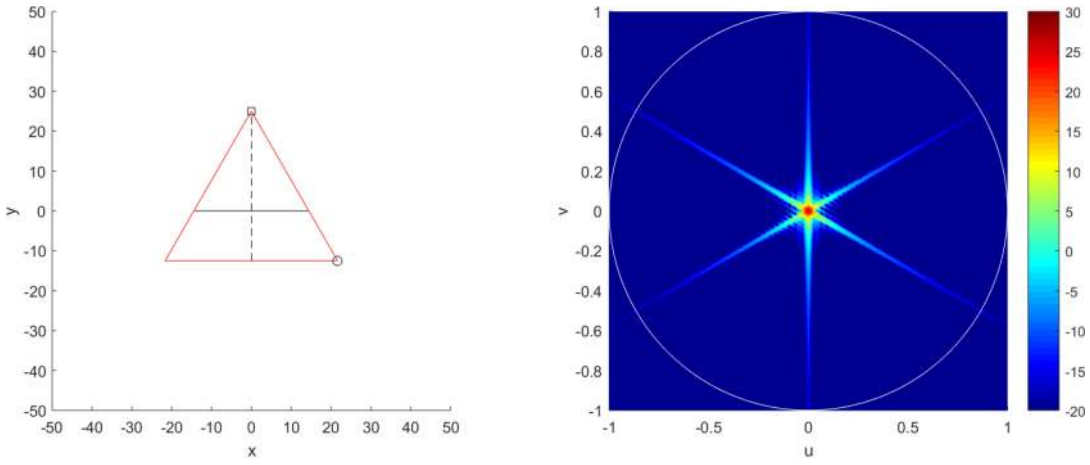

(a) Triangular Aperture geometry (in $[\lambda]$)

(b) $I(\boldsymbol{k})$ for uniform co-phasal illumination (FF [dB])

FIGURE 37. Triangular Aperture, $D_A = 50\lambda$.

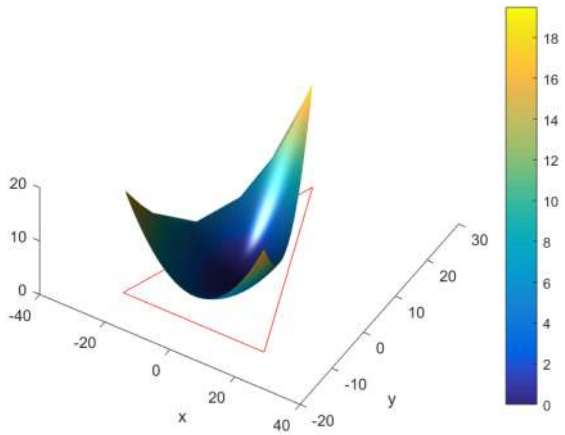

FIGURE 38. Triangular Beam (Phase [rad]), $\lambda_1 = 1, \lambda_2 = 1, \theta = 0°$.

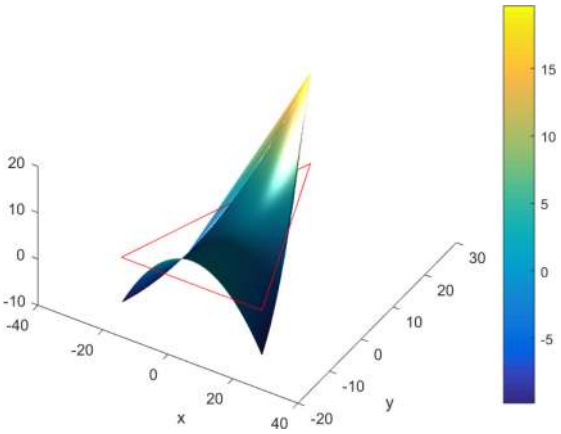

FIGURE 40. Triangular Beam (Phase [rad]), $\lambda_1 = 1, \lambda_2 = -1, \theta = 90°$.

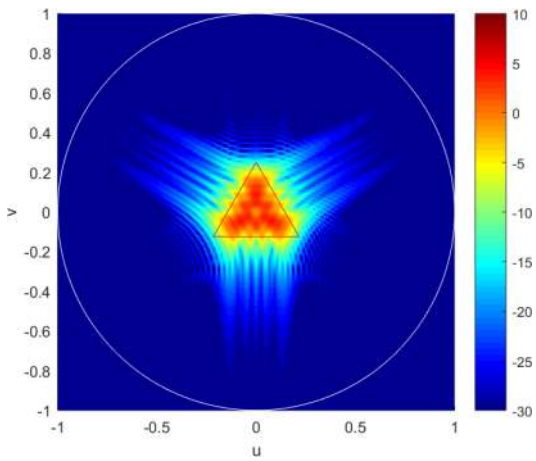

FIGURE 39. Triangular Beam (FF [dB]), $\lambda_1 = 1, \lambda_2 = 1, \theta = 0°$.

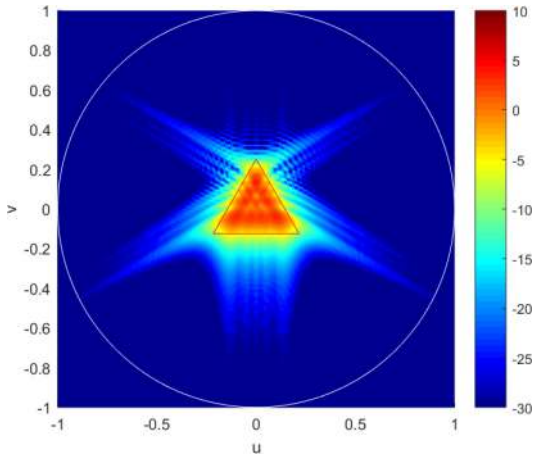

FIGURE 41. Triangular Beam (FF [dB]), $\lambda_1 = 1, \lambda_2 = -1, \theta = 90°$.

The effect of the aperture diameter ($D_A = 25, 100\lambda$) on the quality of the far-field can be appreciated in Fig. 10, while the dependency of the far-field with the beam radius ($u_0 = .2, .6$) for a fixed aperture diameter of 50λ is shown in Fig. 11. Both figures report results for concordant (i.e., a,c) and discordant (i.e., b,d) signs of $\lambda_{1,2}$, respectively.

In a second example we look at generating with the circular aperture of Fig. 5(a) an elliptical beam with 4:1

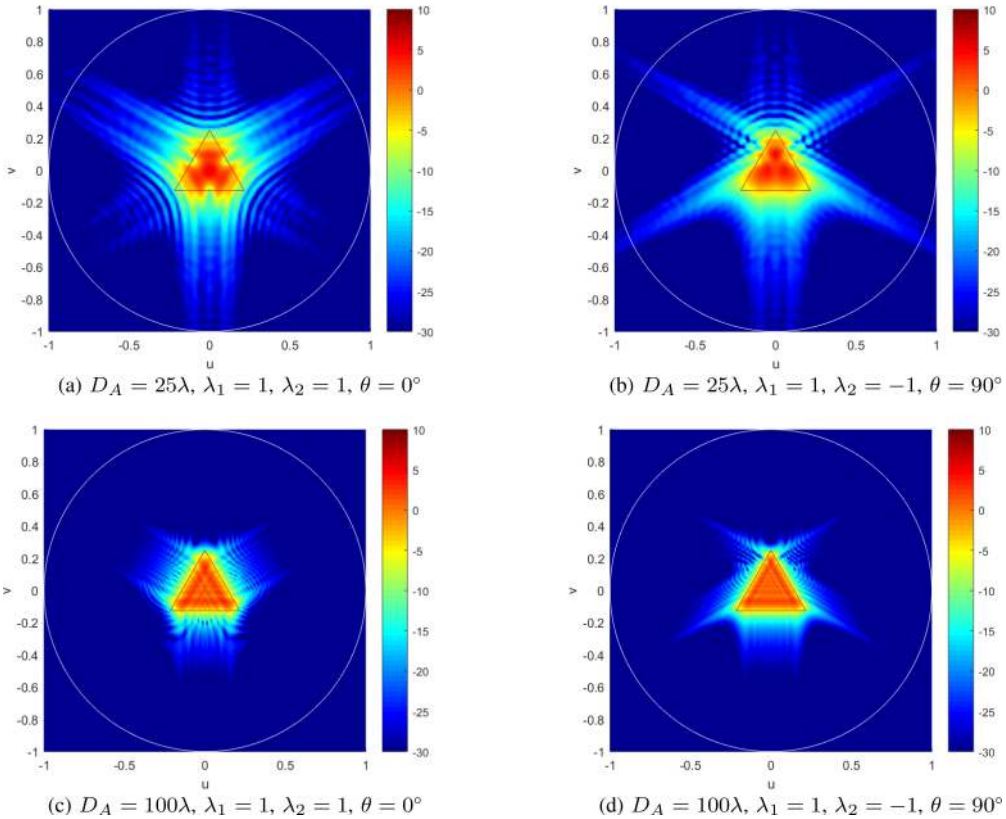

FIGURE 42. Triangular Aperture/Beam - Asymptotic Behaviour, $u_0 = .25$ (FF [dB]).

ratio between the major and minor semi-axes, and the minor semi-axis rotated 45° counter-clockwise with respect to the x-axis. A first suitable mapping correspond to a symmetric affine transformation (42) with parameters $\lambda_1 = 0.5$, $\lambda_2 = 2$, $\theta = 45°$. It corresponds to a first clockwise rotation of the circle $\mathbf{R}(-45°)$ that doesn't change its shape, a contraction along the x-axis of a factor $\lambda_1 = 0.5$, a dilation along the y-axis of a factor $\lambda_2 = 2$, and a final counter-clockwise rotation $\mathbf{R}(45°)$ which aligns the minor semi-axis as desired. The result of the mapping is shown in Fig. 12. The resulting paraboloidal phase and relevant far field are shown in Fig. 13 and Fig. 14, respectively. An alternative mapping with discordant signs can be obtained with the parameters $\lambda_1 = 0.5$, $\lambda_2 = -2$, $\theta = 45°$. The effect of the mapping on the circular aperture is shown in Fig. 15. It gives rise to a hyperbolic paraboloidal phase which is shown in Fig. 16, and to the far-field of Fig. 17.

B. SQUARE APERTURE

A second set of examples is related to square apertures. A square aperture inscribed in a circle of 50λ diameter is assumed (Fig. 18(a)). If uniformly illuminated, the aperture produces the diffraction-limited far-field shown in Fig. 18(b).

As first target we aim at obtaining a square beam of encircling radius $u_0 = 0.25$. Similarly to the circular aperture case, alternative forms of the symmetric affine transformation can be identified corresponding either to concordant or discordant signs of $\lambda_{1,2}$. A paraboloidal phase is obtained with concordant signs (Fig. 19, with far field in Fig. 20), while a hyperbolic paraboloidal phase is obtained with discordant signs (Fig. 21, with far field in Fig. 22).

The effects on the far-field of the aperture diameter ($D_A = 25, 100\lambda$) for an assigned beam radius ($u_0 = .25$), and of the beam radius ($u_0 = .2, .6$) with a given aperture diameter ($D_A = 50\lambda$), can be appreciated in Fig. 23 and Fig. 24, respectively. Also in this case the figures report results for concordant (a,c) and discordant (b,d) signs of $\lambda_{1,2}$.

The possibility of deforming the initial square shape is exemplified in Fig. 25 (with phase in Fig. 26, and far-field in Fig. 27), and of Fig. 28 (with phase in Fig. 29, and far-field in Fig. 30). They can be intuitively understood looking at the diagram (Fig. 4) of the final transformation matrix ($\mathbf{S}$).

The possibility of rotating a square beam generated by a square aperture is first reported in Fig. 31 (map), Fig. 32 (phase [rad]) and Fig. 33(far-field) for an angle of 10°. A rotation of 20° is instead shown in Fig. 34 (map), Fig. 35 (phase [rad]) and Fig. 36 (far-field).

C. TRIANGULAR APERTURE

A third set of examples addresses triangular apertures. A triangular aperture inscribed in a circle of 50λ diameter is assumed (Fig. 37(a)). If uniformly illuminated, the aperture produces the diffraction-limited far-field shown in Fig. 37(b).

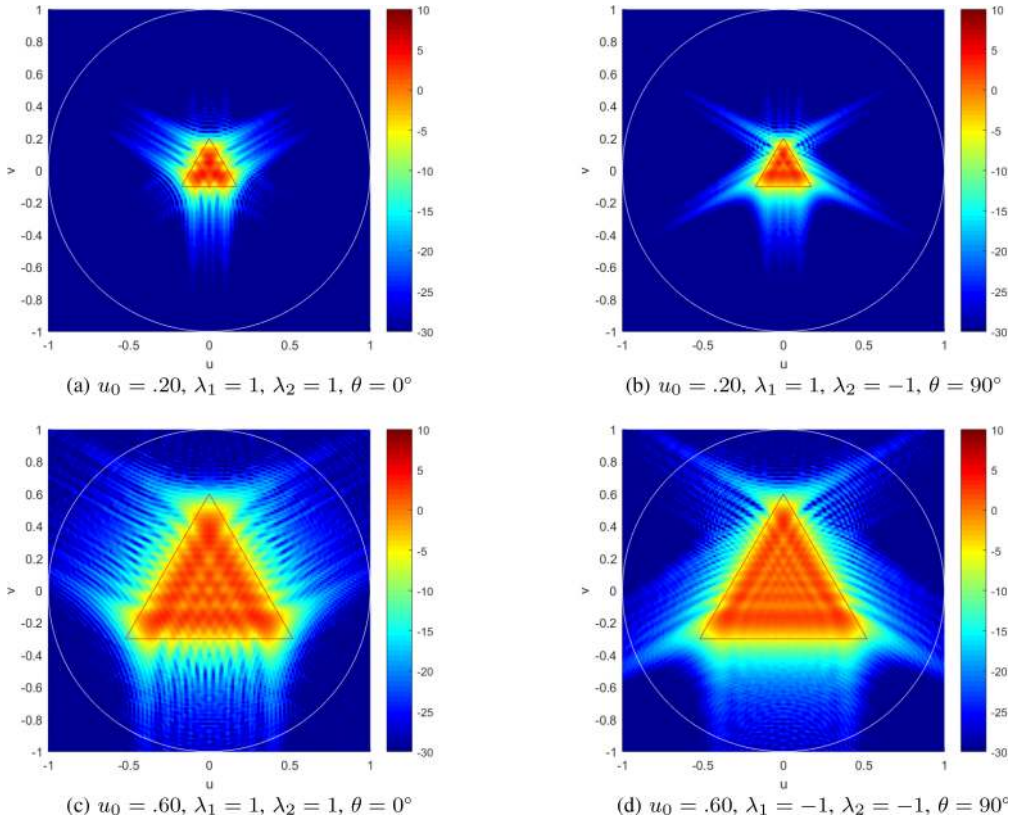

(a) $u_0 = .20,\ \lambda_1 = 1,\ \lambda_2 = 1,\ \theta = 0°$ (b) $u_0 = .20,\ \lambda_1 = 1,\ \lambda_2 = -1,\ \theta = 90°$

(c) $u_0 = .60,\ \lambda_1 = 1,\ \lambda_2 = 1,\ \theta = 0°$ (d) $u_0 = .60,\ \lambda_1 = -1,\ \lambda_2 = -1,\ \theta = 90°$

FIGURE 43. Triangular Aperture/Beam - Beam Zooming Behaviour, $D_A = 50\lambda$ (FF [dB]).

Aiming at obtaining a triangular beam of encircling radius $u_0 = 0.25$, alternative forms of the symmetric affine transformation can be used corresponding either to concordant or discordant signs of $\lambda_{1,2}$. The paraboloidal phase of Fig. 38 is obtained with concordant signs, with far field in Fig. 39. The hyperbolic paraboloidal phase of Fig. 40 is obtained with discordant signs, with far field in Fig. 41).

Effects on the far-field of the aperture diameter ($D_A = 25, 100\lambda$) for an assigned encircled beam radius ($u_0 = .25$), and of the beam radius ($u_0 = .2, .6$) with a given encircling aperture diameter ($D_A = 50\lambda$), can be appreciated in Fig. 42 and Fig. 43, respectively.

The figures report results for concordant (a,c) and discordant (b,d) signs of $\lambda_{1,2}$.

Deformation of the triangular shape is exemplified by the map of Fig. 44 (with phase in Fig. 45, and far-field in Fig. 46, and of Fig. 47 (with phase in Fig. 48, and far-field in Fig. 49).

Triangular beam rotation is reported in Fig. 50 (map), Fig. 51 phase [rad]) and Fig. 52(far-field) for an angle of 10°. While a rotation of 20° is shown in Fig. 53 (map), Fig. 54 (phase [rad]) and Fig. 55 (far-field).

D. ROSE APERTURE

Last set of examples relates to "rose" apertures and beams, these curves have been selected to demonstrate how the asymptotic formulation provide robust results also for apertures with sophisticated shapes. A "rose" curve (also called a rosette or Rhodonea curve) is a plane curve shaped like a petalled flower. They have the following polar representation:

$$x = D_A \cos(N\phi), \quad y = D_A \sin(N\phi)\ . \tag{44}$$

The variable N controls the number of petals, an N-petals rose results for N odd, while a $2N$-petals rose results for N even.

A 8-petals rose aperture inscribed in a circle of 100λ diameter is assumed (Fig. 56(a)). If uniformly illuminated, the aperture produces the diffraction-limited far-field shown in Fig. 56(b).

As first target we aim at obtaining a beam of identical form of the aperture with an encircling radius $u_0 = 0.5$. The paraboloidal phase for concordant signs of $\lambda_{1,2}$ is shown in Fig. 57, with far field in Fig. 58, while the hyperbolic paraboloidal phase for discordant signs of $\lambda_{1,2}$ is shown in Fig. 59, with far field in Fig. 60. In both cases it is interesting to note the accuracy of the far-field in following the shape defined by the aperture.

The effects on the far-field of the aperture diameter ($D_A = 25, 100\lambda$) for an assigned beam radius ($u_0 = .25$), and of the beam radius ($u_0 = .2, .6$) with a given aperture diameter ($D_A = 100\lambda$), can be appreciated in Fig. 61 and Fig. 62, respectively. Also in this case the figures report results for concordant (a,c) and discordant (b,d) signs of $\lambda_{1,2}$.

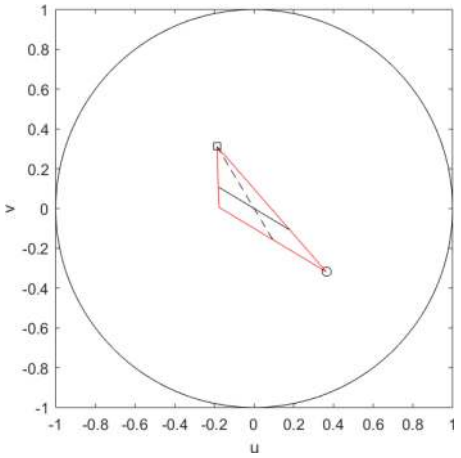

FIGURE 44. Deformed Triangular Beam (Map), $\lambda_1 = 0.5$, $\lambda_2 = 2$, $\theta = 45°$.

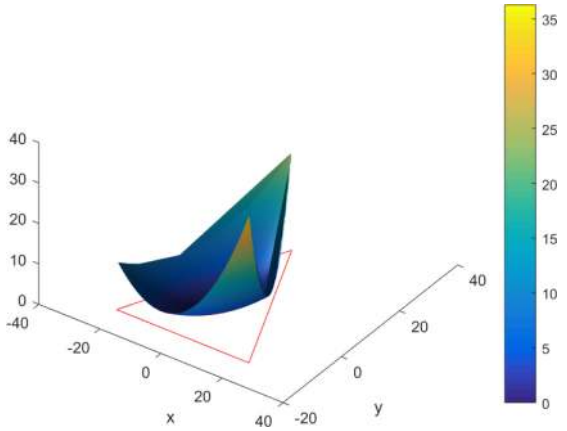

FIGURE 45. Deformed Triangular Beam (Phase [rad]), $\lambda_1 = 0.5$, $\lambda_2 = 2$, $\theta = 45°$.

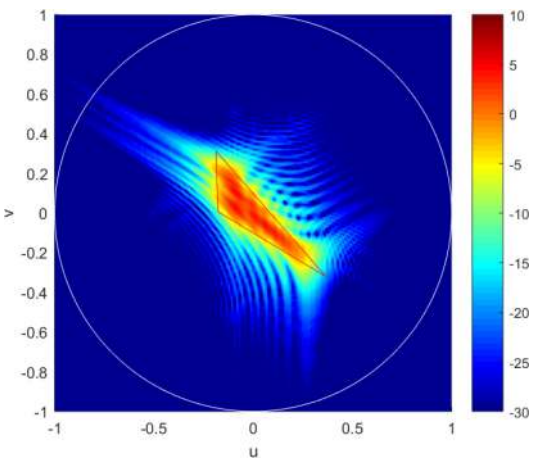

FIGURE 46. Deformed Triangular Beam (FF [dB]), $\lambda_1 = 0.5$, $\lambda_2 = 2$, $\theta = 45°$.

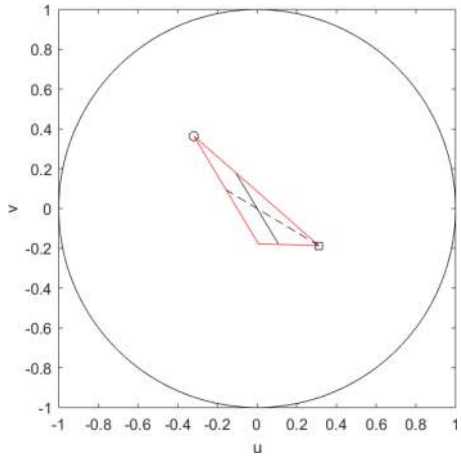

FIGURE 47. Deformed Triangular Beam (Map), $\lambda_1 = 0.5$, $\lambda_2 = -2$, $\theta = 45°$.

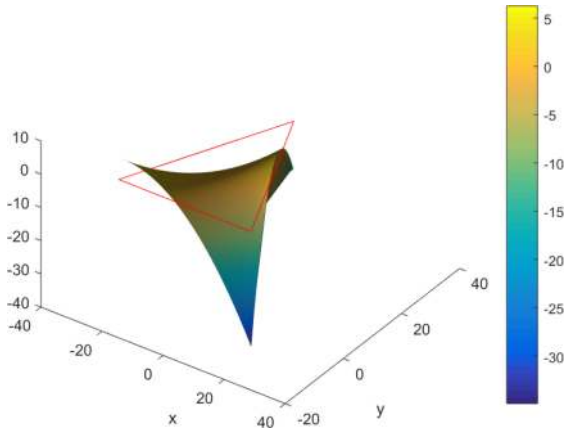

FIGURE 48. Deformed Triangular Beam (Phase [rad]), $\lambda_1 = 0.5$, $\lambda_2 = -2$, $\theta = 45°$.

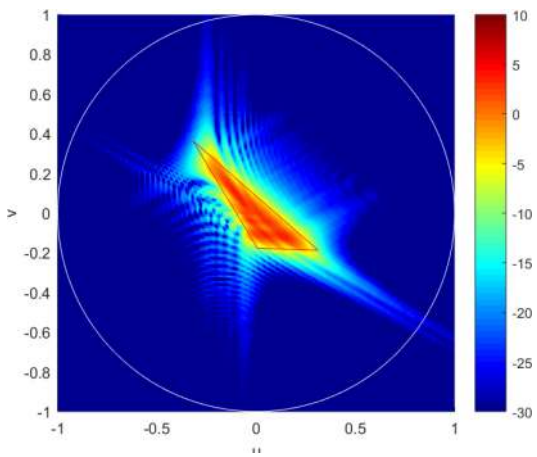

FIGURE 49. Deformed Triangular Beam (FF [dB]), $\lambda_1 = 0.5$, $\lambda_2 = -2$, $\theta = 45°$.

The possibility of deforming the initial rose shape with different choices of the signs of $\lambda_{1,2}$ is exemplified in Fig. 63 (with phase in Fig. 64, and far-field in Fig. 65), and of Fig. 66 (with phase in Fig. 67, and far-field in Fig. 68).

Rotation of the rose beam is finally reported in Fig. 69 (map), Fig. 70 (phase [rad]) and Fig. 71(far-field) for an angle of 2.5°. A rotation of 2.5° is instead shown in Fig. 72 (map), Fig. 73 (phase [rad]) and Fig. 74 (far-field).

VI. CONCLUSION

The paper described how applying the method of stationary phase it is possible to express the asymptotic solution of

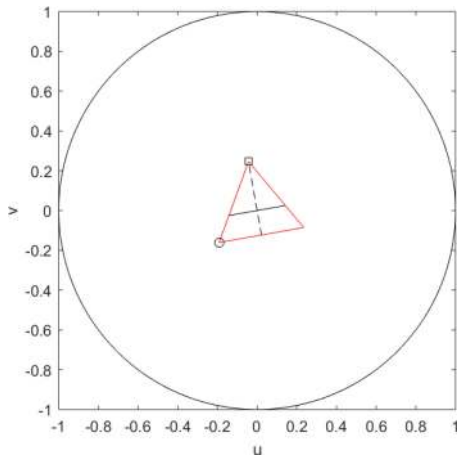

FIGURE 50. Rotated Triangular Beam (Map), $\lambda_1 = 1$, $\lambda_2 = -1$, $\theta = 95°$.

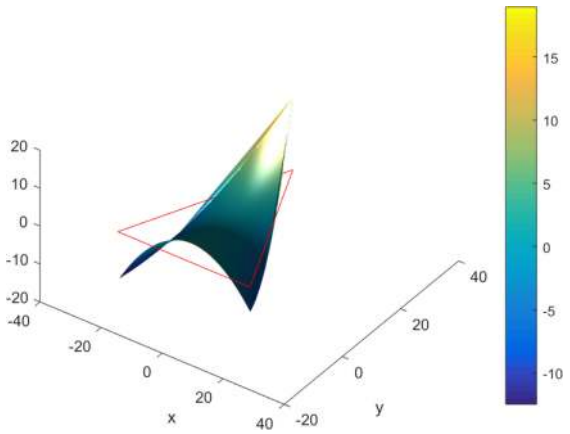

FIGURE 51. Rotated Triangular Beam (Phase [rad]), $\lambda_1 = 1$, $\lambda_2 = -1$, $\theta = 95°$.

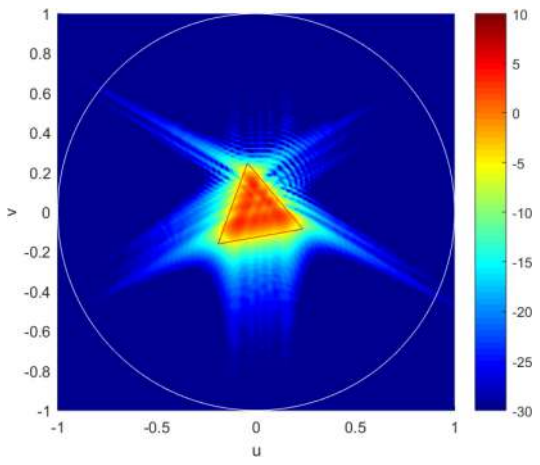

FIGURE 52. Rotated Triangular Beam (FF [dB]), $\lambda_1 = 1$, $\lambda_2 = -1$, $\theta = 95°$.

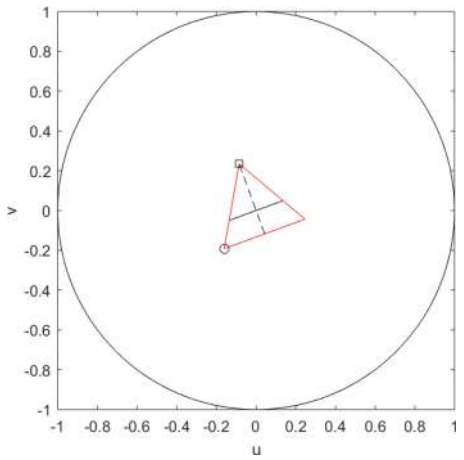

FIGURE 53. Rotated Triangular Beam (Map), $\lambda_1 = 1$, $\lambda_2 = -1$, $\theta = 100°$.

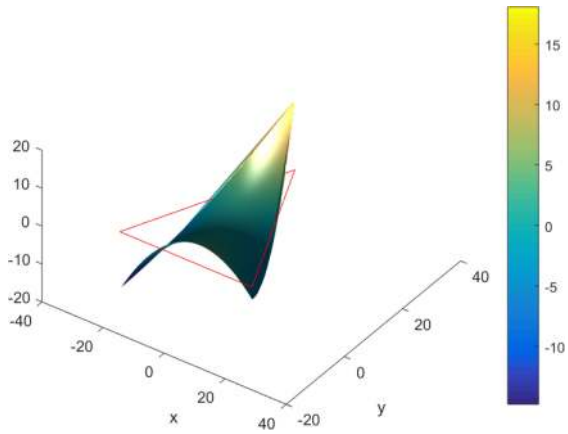

FIGURE 54. Rotated Triangular Beam (Phase [rad]), $\lambda_1 = 1$, $\lambda_2 = -1$, $\theta = 100°$.

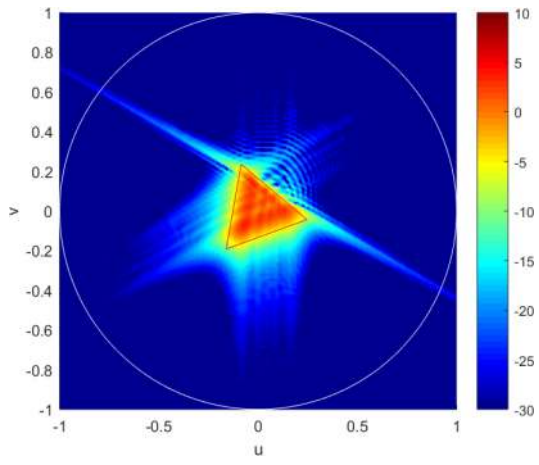

FIGURE 55. Rotated Triangular Beam (FF [dB]), $\lambda_1 = 1$, $\lambda_2 = -1$, $\theta = 100°$.

the problem of phase synthesis of apertures with assigned amplitudes, as a Monge–Ampère partial differential equation (PDE) with appropriate boundary value conditions. It also showed how, introducing an irrotational transport map from the source aperture to the target beam, the Monge–Ampère PDE can be solved in a way similar to Chu's energy mapping principle for reflector shaping, but fulfilling total differentiability. In this Part I paper, it is also proven how irrotational linear maps offer the possibility of obtaining beams of the same shape of the source aperture, a result only observed in the past for circular

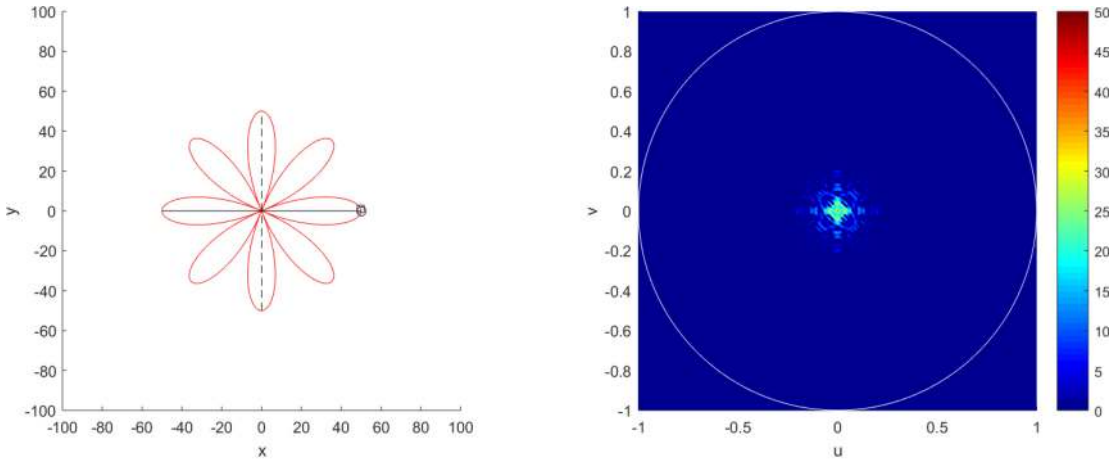

(a) Rose Aperture geometry (in $[\lambda]$)

(b) $I(\boldsymbol{k})$ for uniform co-phasal illumination (FF [dB])

FIGURE 56. Rose Aperture (8 Petals), $D_A = 100\lambda$.

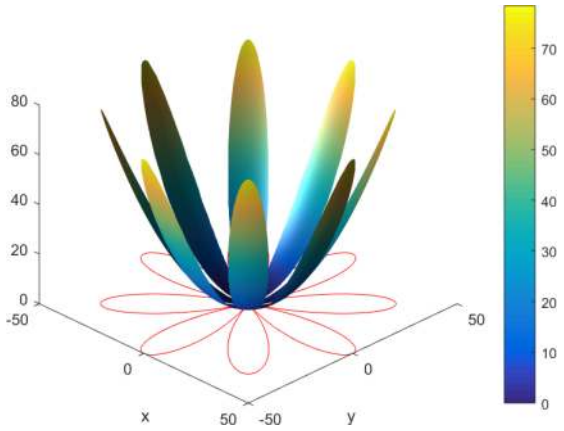

FIGURE 57. Rose Beam (Phase [rad]), $\lambda_1 = 1$, $\lambda_2 = 1$, $\theta = 0°$.

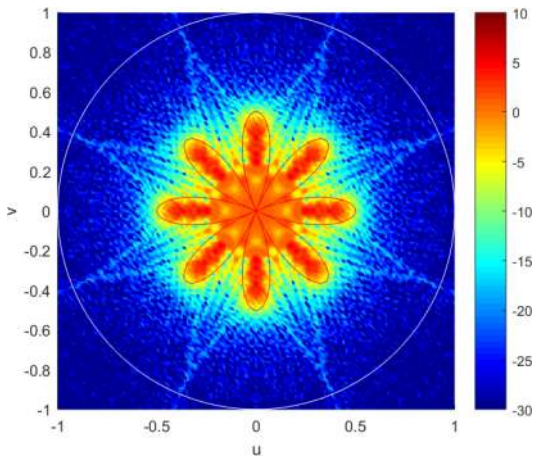

FIGURE 58. Rose Beam (FF [dB]), $\lambda_1 = 1$, $\lambda_2 = 1$, $\theta = 0°$.

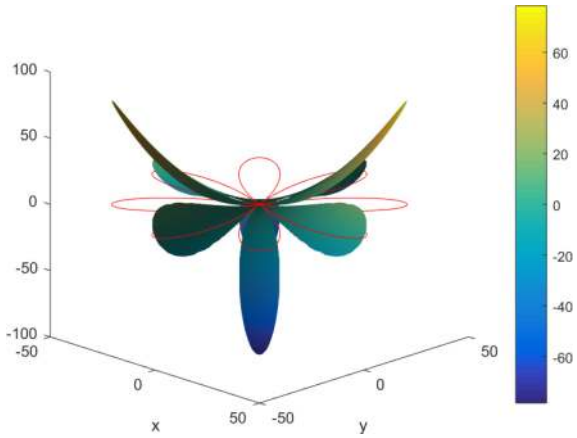

FIGURE 59. Rose Beam (Phase [rad]), $\lambda_1 = 1$, $\lambda_2 = -1$, $\theta = 45°$.

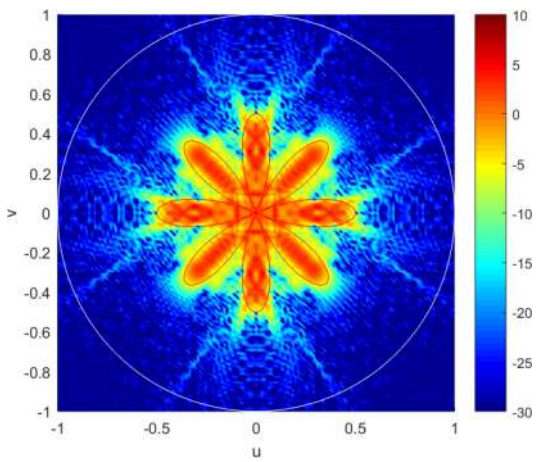

FIGURE 60. Rose Beam (FF [dB]), $\lambda_1 = 1$, $\lambda_2 = -1$, $\theta = 45°$.

and square apertures. Exploiting a polar decomposition of the affine transformation matrix, it has been also demonstrated that the beam can be rotated. In a companion paper [57], the general problem of finding a solution to the Monge–Ampère PDE via irrotational transport maps is addressed and solved by mean of the "optimal transport" theory.

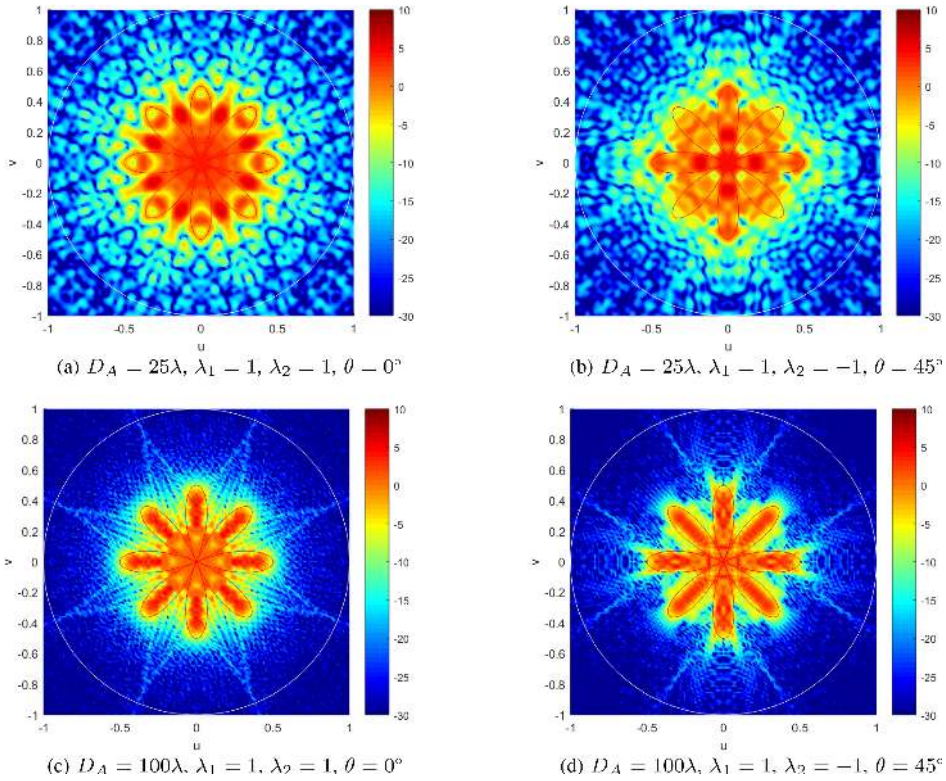

FIGURE 61. Rose Aperture/Beam - Asymptotic Behaviour, $u_0 = .5$ (FF [dB]).

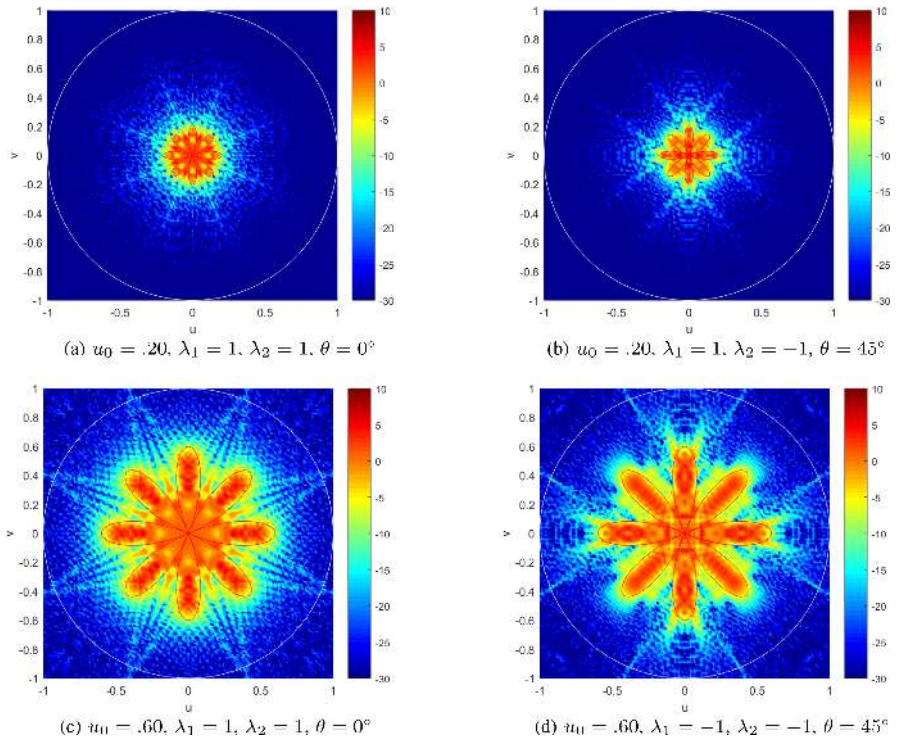

FIGURE 62. Rose Aperture/Beam - Beam Zooming Behaviour $D_A = 100\lambda$ (FF [dB]).

APPENDIX A
STATIONARY PHASE INTEGRAL

In this Appendix we will derive our asymptotic approximation with all details. The calculation can be viewed in the wider context of asymptotic methods in Engineering (see, *e.g.*, [60]). The Fourier integral (1) evaluated in the direction $\boldsymbol{k}_s$, corresponding to the stationary phase condition (4), can be approximated as,

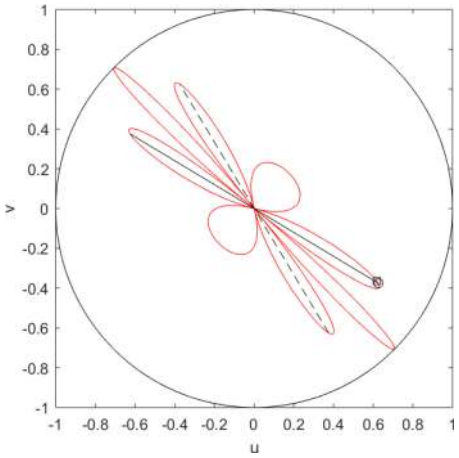

FIGURE 63. Deformed Rose Beam (Map), $\lambda_1 = 0.5$, $\lambda_2 = 2$, $\theta = 45°$.

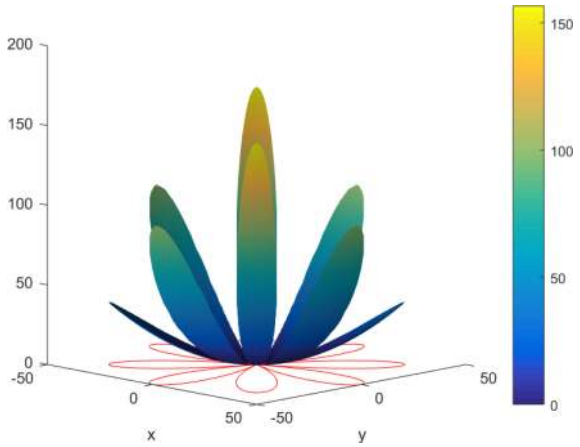

FIGURE 64. Deformed Rose Beam (Phase [rad]), $\lambda_1 = 0.5$, $\lambda_2 = 2$, $\theta = 45°$.

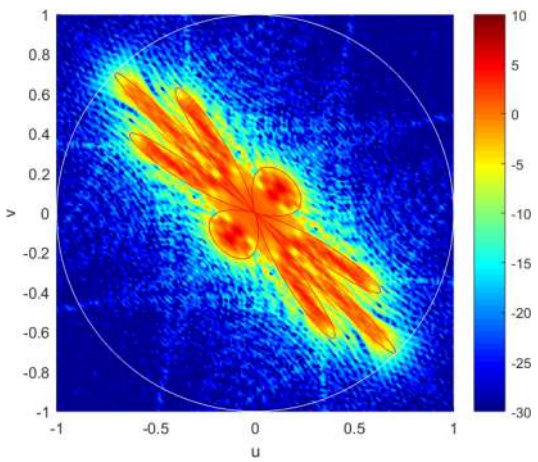

FIGURE 65. Deformed Rose Beam (FF [dB]), $\lambda_1 = 0.5$, $\lambda_2 = 2$, $\theta = 45°$.

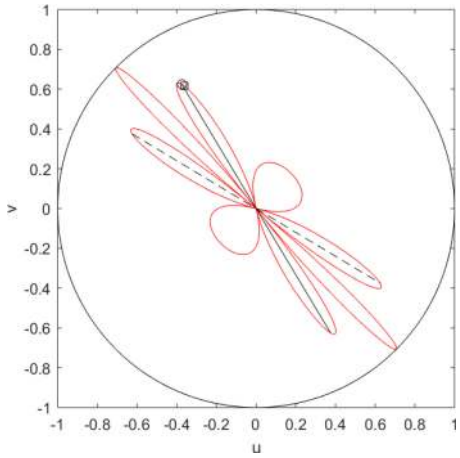

FIGURE 66. Deformed Rose Beam (Map), $\lambda_1 = 0.5$, $\lambda_2 = -2$, $\theta = 45°$.

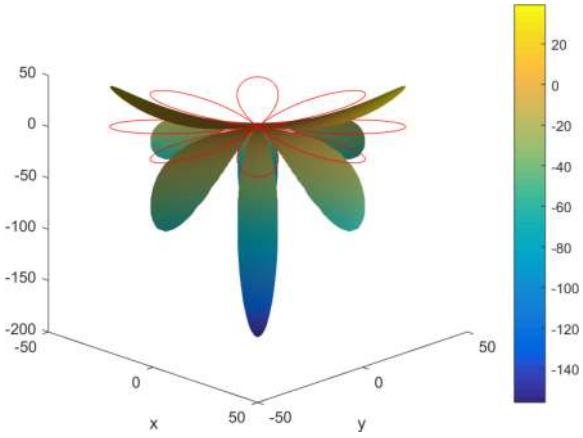

FIGURE 67. Deformed Rose Beam (Phase [rad]), $\lambda_1 = 0.5$, $\lambda_2 = -2$, $\theta = 45°$.

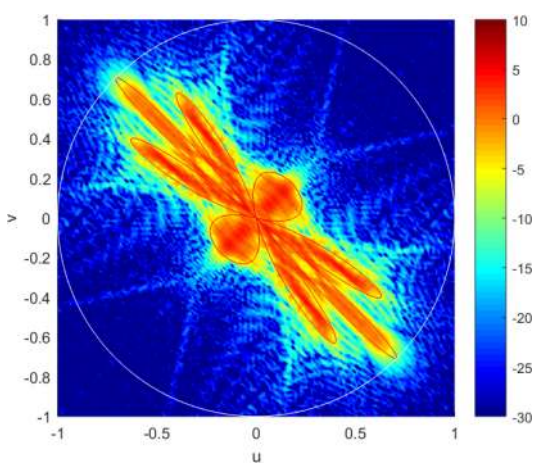

FIGURE 68. Deformed Rose Beam (FF [dB]), $\lambda_1 = 0.5$, $\lambda_2 = -2$, $\theta = 45°$.

$$
\begin{aligned}
&\iint_{\boldsymbol{\Gamma}} f(\boldsymbol{r})\, e^{j\phi(\boldsymbol{r})}\, e^{-j\boldsymbol{k}_s\cdot\boldsymbol{r}}\, d\boldsymbol{r} \\
&\quad\approx f|_{\boldsymbol{r}_s} \iint_{\boldsymbol{\Gamma}} e^{j\left(\phi|_{\boldsymbol{r}_s}+(\boldsymbol{r}-\boldsymbol{r}_s)^T\nabla\phi|_{\boldsymbol{r}_s}+\frac{1}{2}(\boldsymbol{r}-\boldsymbol{r}_s)^T\mathbf{H}\phi|_{\boldsymbol{r}_s}(\boldsymbol{r}-\boldsymbol{r}_s)-\boldsymbol{k}_s\cdot\boldsymbol{r}\right)} d\boldsymbol{r} \\
&\quad= f|_{\boldsymbol{r}_s} e^{j\phi|_{\boldsymbol{r}_s}} \iint_{\mathbb{R}^2} e^{j\left((\boldsymbol{r}-\boldsymbol{r}_s)^T\boldsymbol{k}_s+\frac{1}{2}(\boldsymbol{r}-\boldsymbol{r}_s)^T\mathbf{H}\phi|_{\boldsymbol{r}_s}(\boldsymbol{r}-\boldsymbol{r}_s)-\boldsymbol{k}_s\cdot\boldsymbol{r}\right)} d\boldsymbol{r} \\
&\quad= f|_{\boldsymbol{r}_s} e^{j(\phi|_{\boldsymbol{r}_s}-\boldsymbol{k}_s\cdot\boldsymbol{r}_s)} \iint_{\mathbb{R}^2} e^{j\frac{1}{2}(\boldsymbol{r}-\boldsymbol{r}_s)^T\mathbf{H}\phi|_{\boldsymbol{r}_s}(\boldsymbol{r}-\boldsymbol{r}_s)} d\boldsymbol{r}
\end{aligned}
\tag{45}
$$

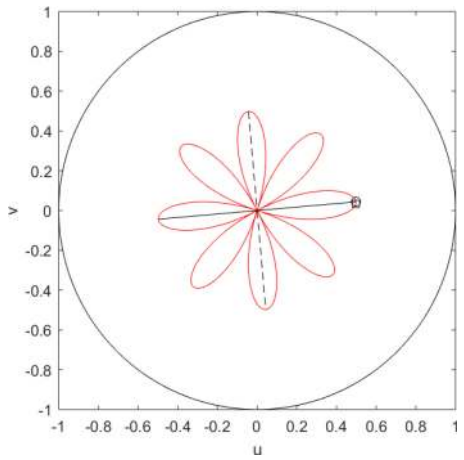

FIGURE 69. Rotated Rose Beam (Map), $\lambda_1 = 1$, $\lambda_2 = -1$, $\theta = 2.5°$.

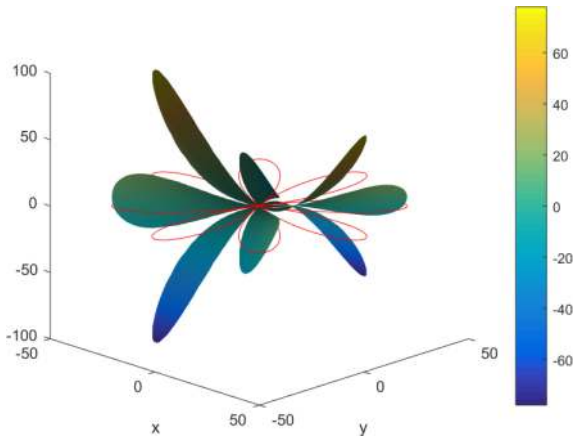

FIGURE 70. Rotated Rose Beam (Phase [rad]), $\lambda_1 = 1$, $\lambda_2 = -1$, $\theta = 2.5°$.

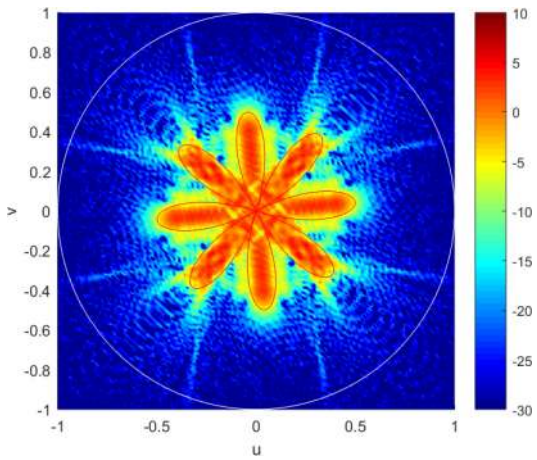

FIGURE 71. Rotated Rose Beam (FF [dB]), $\lambda_1 = 1$, $\lambda_2 = -1$, $\theta = 2.5°$.

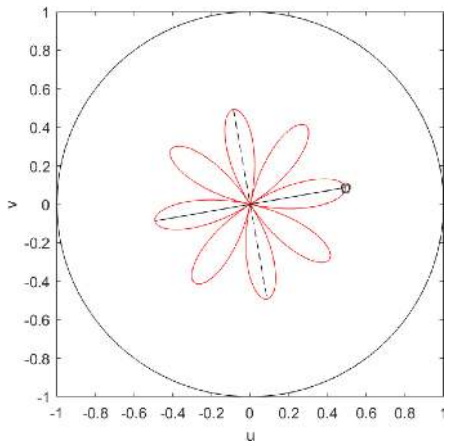

FIGURE 72. Rotated Rose Beam (Map), $\lambda_1 = 1$, $\lambda_2 = -1$, $\theta = 5°$.

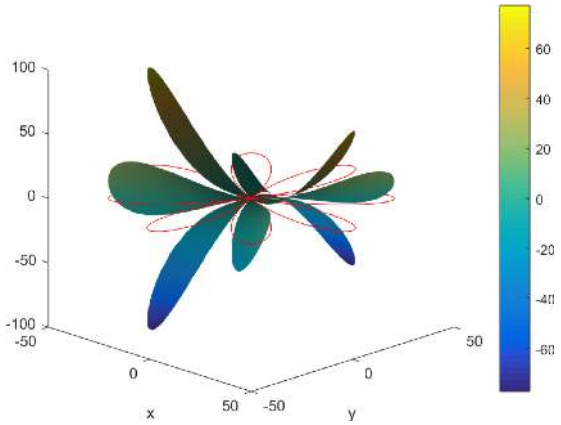

FIGURE 73. Rotated Rose Beam (Phase [rad]), $\lambda_1 = 1$, $\lambda_2 = -1$, $\theta = 5°$.

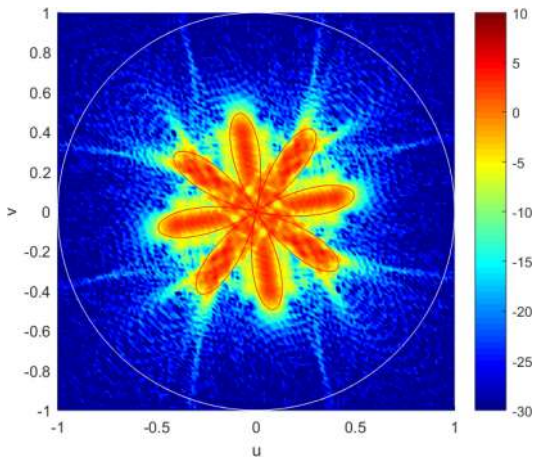

FIGURE 74. Rotated Rose Beam (FF [dB]), $\lambda_1 = 1$, $\lambda_2 = -1$, $\theta = 5°$.

where the integration limits have been extended since the contribution outside the region close to the stationary point can be considered negligible. We can operate a first change of variable $\boldsymbol{r}' = \boldsymbol{r} - \boldsymbol{r}_s$ which simplifies the argument of the complex exponential to $\frac{1}{2}\boldsymbol{r}'^T.\mathbf{H}\phi|_{\boldsymbol{r}_s}\boldsymbol{r}'$. Observing that being the Hessian symmetric (i.e., the matrix and its transpose coincide) the eigenvalues will be real numbers and the matrix orthogonally diagonalizable,

$$P^T \mathbf{H}\phi|_{\boldsymbol{r}_s} P = \mathbf{\Lambda}, \tag{46}$$

we can introduce a second change of variables, $\boldsymbol{r}'' = P^T\boldsymbol{r}'$. The column vectors of P are linearly independent

eigenvectors of the Hessian matrix $.\mathbf{H}\phi|_{\boldsymbol{r}_s}$. They correspond to mutually orthogonal directions which are also known as directions of pure curvature (as along these directions the mixed partial derivatives are null). The eigenvalues λ_1 and λ_2 of the Hessian matrix $.\mathbf{H}\phi|_{\boldsymbol{r}_s}$ are real and provide an information of the local curvature of $\phi(\boldsymbol{r})$ in $\boldsymbol{r}_s$; they are also known as principal curvatures and are invariant under rotation.

The bidimensional integral can be decoupled in two independent monodimensional integrals,

$$\begin{aligned}
&\iint_{\mathbb{R}^2} e^{j\frac{1}{2}(\boldsymbol{r}-\boldsymbol{r}_s)^T \mathbf{H}\phi|_{\boldsymbol{r}_s}(\boldsymbol{r}-\boldsymbol{r}_s)} d\boldsymbol{r} \\
&= \iint_{\mathbb{R}^2} e^{j\frac{1}{2}\boldsymbol{r}'^T \mathbf{H}\phi|_{\boldsymbol{r}_s}\boldsymbol{r}'} d\boldsymbol{r}' \\
&= \iint_{\mathbb{R}^2} e^{j\frac{1}{2}\boldsymbol{r}''^T \Lambda \boldsymbol{r}''} d\boldsymbol{r}'' \\
&= \int_{-\infty}^{\infty} e^{j\frac{1}{2}\lambda_1\xi^2} d\xi \int_{-\infty}^{\infty} e^{j\frac{1}{2}\lambda_2\zeta^2} d\zeta \ . \qquad (47)
\end{aligned}$$

Using the Fresnel integrals identity [61],

$$\int_{-\infty}^{\infty} e^{j\frac{1}{2}ax^2} dx = \sqrt{\frac{2\pi}{|a|}} e^{j\frac{\pi}{4}\text{sign(a)}} \qquad (48)$$

we obtain,

$$F(\boldsymbol{k}_s) \approx f|_{\boldsymbol{r}_s} e^{j(\phi|_{\boldsymbol{r}_s} - \boldsymbol{k}_s\cdot\boldsymbol{r}_s)} \frac{2\pi}{\sqrt{|\lambda_1\lambda_2|}} e^{j\frac{\pi}{4}(\text{sign}(\lambda_1)+\text{sign}(\lambda_2))} \qquad (49)$$

where λ_1 and λ_2 are the real eigenvalues of the Hessian matrix $\mathbf{H}\phi|_{\boldsymbol{r}_s}$.

APPENDIX B
SYMMETRIC MATRICES FACTORIZATION

Let $\mathbf{S}$ be a real symmetric matrix, then the "right polar decomposition" of $\mathbf{S}$ is,

$$\mathbf{S} = \mathbf{UP}, \quad \begin{cases} \mathbf{U} = \mathbf{R}\,\text{sign}(\mathbf{\Lambda})\mathbf{R}^T \\ \mathbf{P} = \mathbf{R}\,\text{abs}(\mathbf{\Lambda})\mathbf{R}^T \end{cases} \qquad (50)$$

where,

$$\mathbf{S} = \mathbf{R}\,\mathbf{\Lambda}\mathbf{R}^T \qquad (51)$$

is the spectral decomposition of $\mathbf{S}$ (also known as Symmetric Schur Decomposition), $\mathbf{\Lambda}$ is a real diagonal matrix, $\mathbf{R}$ is real orthogonal, $\mathbf{R}^{-1} = \mathbf{R}^T$, $\mathbf{U}$ is real unitary (orthogonal), and $\mathbf{P}$ is positive semidefinite. The operators sign( ) and abs( ) must be understood as applied entrywise.

Proof: Being $\mathbf{S}$ real symmetric, $\mathbf{S}^T = \mathbf{S}$, it admits the spectral decomposition (51) (refer to [62, Th. 8.1.1]), with real eigenvalues collected in the diagonal matrix $\mathbf{\Lambda}$ and $\mathbf{R}$ real orthogonal. The real matrix $\mathbf{\Lambda}$ can be then split in sign and modulus and, together with the orthogonality of $\mathbf{R}$, $\mathbf{R}^T\mathbf{R} = I$, it gives:

$$\begin{aligned}
\mathbf{S} &= \mathbf{R}\,\mathbf{\Lambda}\mathbf{R}^T \\
&= \mathbf{R}\,\text{sign}(\mathbf{\Lambda})\text{abs}(\mathbf{\Lambda})\mathbf{R}^T \qquad (52) \\
&= \mathbf{R}\,\text{sign}(\mathbf{\Lambda})\mathbf{R}^T\mathbf{R}\,\text{abs}(\mathbf{\Lambda})\mathbf{R}^T \qquad (53)
\end{aligned}$$

Obviously,

$$\left[\text{sign}(\mathbf{\Lambda})\right]^T \text{sign}(\mathbf{\Lambda}) = \left[\text{sign}(\mathbf{\Lambda})\right]^2 = I \qquad (54)$$

and $\mathbf{U}$ in (55) is a real orthogonal matrix (unitary), as the product of orthogonal matrices is orthogonal. Additionally, the diagonal elements of the diagonal matrix abs($\mathbf{\Lambda}$) correspond to the eigenvalues of $\mathbf{P}$ in (55). Being them all positive, the matrix $\mathbf{P}$ is positive semidefinite. The matrices $\mathbf{U}$ and $\mathbf{P}$ correspond to "Orthogonal Polar Factor" and "Symmetric Polar Factor", respectively, of the polar decomposition of real matrices (refer to [62, Th. 9.4.1]).

It is worth mentioning that the intermediate result (52) can be interpreted as the Singular Value Decomposition of the real matrix $\mathbf{S}$ (refer to [62, Th. 2.4.1]),

$$\mathbf{S} = \mathbf{V}\mathbf{\Sigma}\mathbf{W}^T, \quad \begin{cases} \mathbf{\Sigma} = \text{abs}(\mathbf{\Lambda}) \\ \mathbf{V} = \mathbf{R}\,\text{sign}(\mathbf{\Lambda}) \\ \mathbf{W} = \mathbf{R} \end{cases} \qquad (55)$$

If the singular values abs($\mathbf{\Lambda}$) are arranged in descending order, the matrices $\mathbf{V}$ and $\mathbf{W}$ are unique up to a sign change of homologous columns of $\mathbf{V}$ and $\mathbf{W}$. This gives freedom in selecting the signs of the columns of the matrix $\mathbf{R}$ such that $\det(\mathbf{R}) = 1$, and the matrix can be represented as a rotation matrix,

$$\mathbf{R} = \mathbf{R}(\theta) = \begin{bmatrix} \cos\theta & -\sin\theta \\ \sin\theta & \cos\theta \end{bmatrix} \qquad (56)$$

Combining together the above results, we obtain the following form for the decomposition of the symmetric $\mathbf{S}$ (2×2) real matrix,

$$\mathbf{S} = \mathbf{R}(\theta)\begin{bmatrix} \text{sign}(\lambda_1) & 0 \\ 0 & \text{sign}(\lambda_2) \end{bmatrix}\begin{bmatrix} |\lambda_1)| & 0 \\ 0 & |\lambda_2| \end{bmatrix}\mathbf{R}(-\theta) \qquad (57)$$

REFERENCES

[1] R. C. Spencer, "Synthesis of microwave diffraction patterns with application to CSC ^{2} patterns," MIT Radiat. Lab., Lexington, MA, USA, Rep. 54-24, Jun. 1943.

[2] D. W. Fry, "Some recent developments in the design of centimetric aerial systems," *J. Inst. Electr. Eng. Part IIIA, Radioloc.*, vol. 93, no. 10, pp. 1497–1510, 1946, doi: 10.1049/ji-3a-1.1946.0254.

[3] L. J. Chu, "Microwave beam-shaping antenna," Res. Lab. Electron., Cambridge, MA, USA, MIT Technical Rep. N. 40, Jun. 1947.

[4] L.C. Van Atta, T.J. Keary, "Shaped-beam antennas," in *Microwave Antenna Theory and Design*, S. Silver, Eds., Columbus, OH, USA: McGraw–Hill, 1949.

[5] A. S. Dunbar, "On the theory of antenna beam shaping," *J. Appl. Phys.*, vol. 23, no. 8, pp. 847–853, Aug. 1952.

[6] J. S. Ajioka and H. A. Rosen, "Shaped beam antenna," U.S. Patent 3 680 143, Jul. 1970.

[7] P. Neyret, "Antenna technology at INTELSAT," *Annales des Telecommun.*, vol. 40, nos. 7–8, pp. 331–377, 1985.

[8] J. H. Cowan and P. J. Wood, "A shaped beam dual polarization antenna for a regional satellite communication system," in *Proc. 3rd Eur. Microw. Conf.*, 1973, pp. 1–4, doi: 10.1109/EUMA.1973.331692.

[9] J. H. Cowan, P. J. Wood, R. W. Ashton, and T. G. Boswell, "Design and development of SHF dual polarisation offset-fed reflector antennas," MSDS report Y/226/9345 on ESTEC contract 2130/73 JS, 1975.

[10] T. Katagi and Y. Takeichi, "Shaped-beam horn-reflector antennas," *IEEE Trans. Antennas Propag.*, vol. 23, no. 6, pp. 757–763, Nov. 1975, doi: 10.1109/TAP.1975.1141194.

[11] E. Amyotte and L. Martins Camelo, "Antennas for satellite communications," in *Space Antenna Handbook*, W. A. Imbriale, S. Gao, and L. Boccia, Eds., Hoboken, NJ, USA: Wiley, 2012.

[12] P. Balling, "Wavefront synthesis of contoured beam antennas with low cross-polarisation," TICRA ApS, Copenhagen, Denmark, Rep. S-92-01, Jun. 1979.

[13] R. Jorgensen, "Coverage shaping of contoured-beam antennas by aperture field synthesis," *IEE Proc. H, Microw., Antennas Propag.*, vol. 127, no. 4, pp. 201–208, Aug. 1980.

[14] C. E. Cook, "Pulse compression—Key to more efficient radar transmission," *Proc. IRE*, vol. 48, no. 3, pp. 310–316, Mar. 1960.

[15] E. L. Key, E. N. Fowle, and R. D. Haggarty, "A method of designing signals of large time-bandwidth product," *Proc. IRE Int. Con. Rec.*, vol. 4, pp. 146–154, Mar. 1961.

[16] E. N. Fowle, "The design of FM pulse compression signals," *IEEE Trans. Inf. Theory*, vol. 10, no. 1, pp. 61–67, Jan. 1964.

[17] G. Cui, A. De Maio, A. Farina, and J. Li, Eds., *Radar Waveform Design Based on Optimization Theory*. London, U.K.: Inst. Eng. Technol., 2020.

[18] A. Chakraborty, B. Das, and G. Sanyal, "Beam shaping using nonlinear phase distribution in a uniformly spaced array," *IEEE Trans. Antennas Propag.*, vol. 30, no. 5, pp. 1031–1034, Sep. 1982.

[19] R. Kinsey, "Phased array beam spoiling technique," in *Proc. IEEE Antennas Propag. Soc. Int. Symp.*, vol. 2, 1997, pp. 698–701.

[20] J. O. Coleman, D. P. Scholnik, and K. R. McPhail, "Phase-only tapers for regular planar arrays a heuristic nonlinear-FM approach," in *Proc. IEEE Int. Symp. Phased Array Syst. Technol. (ARRAY)* 2010, pp. 113–120.

[21] J. F. Bull, P. Kalkata, and C. E. Profera, "Application of the method of steepest descent optimization to the design of shaped beam antennas," in *Proc. Antennas Propag. Soc. Int. Symp.*, May 1982, pp. 600–603.

[22] A. Cherrette and D. Chang, "Phased array contour beam shaping by phase optimization," in *Proc. Antennas Propag. Soc. Int. Symp.*, Jun. 1985, pp. 475–478.

[23] O. M. Bucci, G. D'Elia, G. Mazzarella, and G. Panariello, "Antenna pattern synthesis: A new general approach," *Proc. IEEE*, vol. 82, no. 3, pp. 358–371, Mar. 1994.

[24] A. Capozzoli, C. Curcio, A. Liseno, and G. Toso, "Fast, phase-only synthesis of aperiodic reflectarrays using NUFFTs and CUDA," *Progr. Electromagn. Res.*, vol. 156, pp. 83–103, Jan. 2016.

[25] O. O. Bulatsyk, B. Z. Katsenelenbaum, Y. P. Topolyuk, and N. N. Voitovich, *Phase Optimization Problems. Application in Wave Field Theory*, Hoboken, NJ, USA: Wiley, 2010.

[26] M. I. Andriychuk, "Synthesis of antenna systems according to the desired amplitude radiation characteristics," in *Numerical Simulations—From Theory to Industry*, M. Andriychuk, Eds., Rang-du-Fliers, France: InTech, 2012. pp. 191–218.

[27] K.K. Yan and Y. Lu, "Sidelobe reduction in array-pattern synthesis using genetic algorithm," *IEEE Trans. Antennas Propag.*, vol. 45, no. 7, pp. 1117–1122, Jul. 1997.

[28] D. W. Boeringer, D. H. Werner, and D. W. Machuga, "A simultaneous parameter adaptation scheme for genetic algorithms with application to phased array synthesis," *IEEE Trans. Antennas Propag.*, vol. 53, no. 1, pp. 356–371, Jan. 2005.

[29] D. Gies, Y. Rahmat-Samii, "Particle swarm optimization for reconfigurable phase-differentiated array design," *Microw. Opt. Technol. Lett.*, Vol. 38, No. 3, pp. 168–175, Aug. 2003.

[30] S. Selleri, M. Mussetta, P. Pirinoli, R. E. Zich, and L. Matekovits, "Differentiated meta-PSO methods for array optimization," *IEEE Trans. Antennas Propag.*, vol. 56, no. 1, pp. 67–75, Jan. 2008.

[31] E. Agastra, G. Pelosi, S. Selleri, and R. Taddei, "Taguchi's method for multi-objective optimization problems," *Int. J. RF Microw. Comput.-Aided Eng.*, Vol. 23, No. 3, pp. 357–366, May 2013.

[32] M. H. Weatherspoon, J. D. Connor, and S. Y. Foo, "Shaped beam synthesis of phased arrays using the cross entropy method," *Int. J. Numer. Model., Electron. Netw., Devices Fields*, vol. 26, no. 6, pp. 630–642, 2013.

[33] P. Angeletti, L. Berretti, S. Maddio, G. Pelosi, S. Selleri, and G. Toso, "Phase-only synthesis for large planar arrays via zernike polynomials and invasive weed optimization," *IEEE Trans. Antennas Propag.*, vol. 70, no. 3, pp. 1954–1964, Mar. 2022, doi: 10.1109/TAP.2021.3119113.

[34] A. Papoulis, *The Fourier Integral and its Applications*. New York, NY, USA: McGraw-Hill, 1962.

[35] G. N. Watson, "The limits of applicability of the principle of stationary phase," *Proc. Cambridge Philos. Soc.*, vol. 19, pp. 49–55, 1918.

[36] G. G. Stokes, "On the numerical calculation of a class of definite integrals and infinite series," *Cambridge Philos. Trans.*, vol. 9, pp. 166–187, 1856.

[37] W. Thompson, "On the waves produced by a single impulse in water of any depth, or in a dispersive medium," *Proc. R. Soc.*, vol. 42, pp. 80–83, Dec. 1887.

[38] J. G. Van Der Corput, "Zur Methode der stationären phase. Erste Mitteilung, Einfache Integrale," *Compositio Math.*, vol. 1, pp. 15–38, 1934.

[39] J. G. Van Der Corput, "Zur Methode der stationären phase, Zweite Mitteilung, Wiederum einfache Integrale," *Compositio Math.*, vol. 3, pp. 328–372, 1936.

[40] J. G. Van Der Corput, "On the methods of critical points I," *Proc. Ned. Acad. Wetensch.*, vol. 51, 1948.

[41] A. Erdelyi, "Asymptotic representations of Fourier integrals and the method of stationary phase," *J. Soc. Indust. Appl. Math.*, vol. 3, no. 1, pp. 17–27, 1955.

[42] A. Erdelyi, *Asymptotic Expansions*. New York, NY, USA: Dover Publ., 1956.

[43] N. G. de Bruijn. *Asymptotic Methods in Analysis* (Bibliotheca Mathematica). vol. 4. Amsterdam, The Netherlands: North-Holland Publ. Co., 1958.

[44] S. Nomoto, "Synthesis of curved fan-beams by generalized theory of doubly curved reflectors," *Electron. Commun. Japan, Part I, Commun.*, vol. 87, no. 12, pp. 39–48, Sep. 2004, doi: 10.1002/ecja.10219.

[45] J. S. Schruben, "Formulation of a reflector-design problem for a lighting fixture," *J. Opt. Soc. America*, vol. 62, no. 12, pp. 1498–1501, Dec. 1972.

[46] B. S. Westcott and A. P. Norris, "Reflector synthesis for generalized far-fields," *J. Phys. A, Math. Gener.*, vol. 8, no. 4, pp. 521–532, Apr. 1975.

[47] B. S. Westcott, *Shaped Reflector Antenna Design*. Hertfordshire, U.K.: Res. Stud. Press LTD., 1983.

[48] G. Monge, *Mémoire sur le calcul intégral des équations aux différences partielles*, Mémoires de l'Académie des Sciences, De l'Imprimerie royale, Paris, France, 1784.

[49] A.-M. Ampère, *Mémoire contenant l'application de la théorie exposée dans le XVII. e Cahier du Journal de l'École polytechnique, à l'intégration des équations aux différentielles partielles du premier et du second ordre*, De l'Imprimerie royale, Paris, France, 1819.

[50] A. V. Pogorelov, *Monge–Ampère Equations of Elliptic Type*, P. Noordhoff Ltd., Groningen, The Netherlands, 1964.

[51] A. Figalli, *The Monge–Ampère Equation and Its Applications* (Zurich Lectures in Advanced Mathematics). Helsinki, Finland: Eur. Math. Soc., 2017.

[52] J. Urbas, "On the second boundary value problem for equations of Monge-Ampère type," *J. Reine Angew. Math.*, vol. 487, pp. 115–124, 1997.

[53] N. Trudinger and X.-J. Wang, "On the second boundary value problem for Monge-Ampère type equations and optimal transportation," *Annali della Scuola Normale Superiore di Pisa—Classe di Scienze, Serie 5*, vol. 8, no. 1, pp. 143–174, 2009.

[54] B. Cleaveland, "Flat-topped beams from a uniform amplitude rectangular aperture," in *Proc. IEEE Antennas Propag. Soc. Int. Symp.*, 1997, pp. 686–689, doi: 10.1109/APS.1997.631554.

[55] A. V. Shishlov, Y. V. Krivosheev, and V. I. Melnichuk, "Principal features of contour beam phased array antennas," in *Proc. IEEE*

Int. Symp. Phased Array Syst. Technol. (PAST), 2016, pp. 1–8, doi: 10.1109/ARRAY.2016.7832635.
[56] G. Monge, "Mémoire sur la théorie des déblais et des remblais," Histoire de l'Académie royale des sciences avec les mémoires de mathématique et de physique tirés des registres de cette Académie, pp. 666–705, 1781.
[57] P. Angeletti, G. Toso, and R. Vitolo, "Asymptotic phase synthesis by transport maps—Part II: optimal transport problem," *IEEE Open J. Antennas Propag.*, vol. 7, no. 2, pp. 369–393, Apr. 2026, doi: 10.1109/OJAP.2025.3646973.
[58] M. Born and E. Wolf, *Principles of Optics: Electromagnetic Theory of Propagation, Interference and Diffraction of Light*, 7th ed. Cambridge, U.K.: Cambridge Univ., 1999.
[59] T. M. Apostol, *Calculus, Volume II, Multi Variable Calculus and Linear Algebra, with Applications to Differential Equations and Probability*, 2nd ed. New York, NY, USA: Wiley, 1969.
[60] G. Fikioris, I. Tastsoglou, and O. N. Bakas, *Selected Asymptotic Methods with Applications to Electromagnetics and Antennas* (Synthesis Lectures on Computational Electromagnetics), vol. 31. San Rafael, CA, USA: Morgan Claypool Publ., 2013.
[61] "Fresnel integrals." Wolfram MathWorld. Accessed: Dec. 31, 2025. [Online]. Available: https://mathworld.wolfram.com/FresnelIntegrals.html
[62] G. H. Golub and C. F. Van Loan, *Matrix Computations*, 4th ed. Baltimore, MD, USA: Johns Hopkins Univ., 2012.

PIERO ANGELETTI (Senior Member, IEEE) received the Laurea degree (summa cum laude) in electronics engineering from the University of Ancona, Italy, in 1996, and the Ph.D. degree in electromagnetism from the University of Rome "La Sapienza," Italy, in 2010. Since 2004, he has been with the European Space Research and Technology Center of the European Space Agency (ESA), Noordwijk, The Netherlands. He has been recently appointed as the Head of the Secure Connectivity Space Segment Office, with responsibility for the ESA design, development and deployment activities related to Infrastructure for Resilience, Interconnectivity and Security by Satellite multiconstellations space segment. His 25+ years experience in RF Systems engineering and technical management encompasses conceptual/architectural design, tradeoff, detailed design, production, integration and testing of satellite payloads and active antenna systems for commercial/military telecommunications and navigation (spanning all the operating bands and set of applications) as well as for multifunction RADARs and electronic counter measure systems. This has been acquired through direct industrial experience in several aerospace companies (i.e., Agusta-Westland, Thales Alenia Space, Boeing, Elettronica, and Airbus Defence and Space) in different job roles (research and development, innovation, production, procurement, and integration) and matured in the privileged position at the ESA, at the cross-road of all major European developments. He authored/co-authored over 300 technical reports, book chapters and papers published in peer reviewed professional journals and international conferences' proceedings. He holds several patents related to satellite payload and antenna technology. Together with Dr. G. Toso, he is an Instructor of the course on "Multibeam Antennas and Beamforming Networks" which, since 2012, has been offered at main IEEE and European microwaves, wireless and antenna conferences (IEEE APS, IEEE IMS, EuMW, EuCAP, IEEE ICWITS, and ESA Internal University). Together they also organize the EurAP-ESoA course on Active Antennas in 2021, 2023, and 2025. In 2022, he received the S. A. Schelkunoff Award by the IEEE Antennas and Propagation Society for the Best IEEE TAP Paper published in 2021, and in 2023, he has been appointed IEEE MTT-S and AP-S Inter-Society Distinguished Lecturer by the Inter-Society Committee of the IEEE MTT and AP societies.

GIOVANNI TOSO (Fellow, IEEE) received the Laurea degree (cum laude) and Ph.D. degree from the University of Florence, Italy, in 1992 and 1995, respectively, where he was a Postdoctoral Fellowship in 1999. Since 2000, he has been with the Antenna and Submillimeter Waves Section, European Space Agency (ESA), European Space Research and Technology Centre, Noordwijk, The Netherlands. He has been initiating research and development activities on satellite antennas based on arrays, reflectarrays, discrete lenses, and reflectors. He has promoted the development of the commercial software tool QUPES by TICRA, currently used worldwide, for the analysis and design of periodic and quasi-periodic surfaces, such as reflectarrays, frequency selective surfaces, transmitarrays, and polarizers. He received, together with Prof. A. Skrivervik, the European School of Antennas Best Teacher Award in 2018. In 2014, he has been a Guest Editor, together with Dr. R. Mailloux, of the Special Issue on "Innovative Phased Array Antennas Based on Non-Regular Lattices and Overlapped Subarrays" published in the IEEE TRANSACTIONS ON ANTENNAS AND PROPAGATION and, for the IEEE Antennas and Propagation Society, was an Associate Editor from 2013 to 2016. In 2018, he has been the Chairperson of the 39th ESA Antenna Workshop on "Multibeam and Reconfigurable Antennas." Since 2010, together with Dr. P. Angeletti, he has been instructing short courses on multibeam antennas and beamforming networks during international conferences that have been attended by more than 1300 participants. Together with Dr. P. Angeletti, he is the organizer of the EurAAP-ESoA Course on Active Antennas. Together with Dr. E. Gandini, he is also the organizer of the EurAAP-ESoA Course on Satellite Antennas. Since January 2023, he has been elevated to IEEE Fellow grade for contributions to multibeam antenna developments for satellite applications. He is a Distinguished Lecturer of the IEEE Antennas and Propagation Society.

RAFFAELE VITOLO received the degree in mathematics from the University of Camerino in 1991, and the Ph.D. degree in mathematics from the University of Florence in 1996.

He became an Assistant Professor with the Dipartimento di Matematica, Università di Lecce from 1998 to 2003, then has been an associate professor and a full professor since 2024. He is a member of the Istituto Nazionale di Alta Matematica (Section of Mathematical Physics–GNFM) and of the Istituto Nazionale di Fisica Nucleare (INFN, Section of Lecce). He has been teaching since 1995 about 2–3 courses per year on basic mathematics, mathematical physics, applied mathematics, mostly with the Università del Salento, where he is an advisory board member of some Ph.D. programmes. He has been an adviser or a co-adviser for several Ph.D. student in mathematics. He is the author of more than 60 papers in refereed international high-level journals in pure mathematics, applied mathematics, theoretical physics (indexed in Scopus and Web of Science) and of one research-oriented book published by Springer. In the framework of a collaboration with the European Space Agency, he is a co-inventor of a patent. He has been a co-author of researchers from Universities in Canada, Czech Republic, Germany, Italy, The Netherlands, Russia, Spain, U.K., Ukraine, and USA. He was a speaker at about 30 international conferences (invited in many of them) in Europe and Russia. He was one of the organizers of about 15 international conferences. He was a member of more than 20 funded research project. He is the national responsible of the INFN Project Mathematical Methods in non-linear physics, involving over 40 researchers from all over Italy. His research interest are: geometric methods in partial differential equations, integrable systems, symbolic computations and Lisp programming, applied and industrial mathematics, and numerical computations in MATLAB.